MODELING AIR QUALITY NEAR FREEWAYS USING A THREE DIMENSIONAL EULERIAN MODEL

A Thesis

by

SRI HARSHA KOTA

Submitted to the Office of Graduate Studies of
Texas A&M University
in partial fulfillment of the requirements for the degree of

MASTER OF SCIENCE

August 2009

Major Subject: Civil Engineering

MODELING AIR QUALITY NEAR FREEWAYS USING A THREE DIMENSIONAL EULERIAN MODEL

A Thesis

by

SRI HARSHA KOTA

Submitted to the Office of Graduate Studies of
Texas A&M University
in partial fulfillment of the requirements for the degree of

MASTER OF SCIENCE

Approved by:

Chair of Committee, Qi Ying
Committee Members, Bill Batchelor
Renyi Zhang
Head of Department, David V Rosowsky

August 2009

Major Subject: Civil Engineering

ABSTRACT

Modeling Air Quality Near Freeways Using a Three Dimensional Eulerian Model.

(August 2009)

Sri Harsha Kota, B.E., Chaitanya Bharathi Institute of Technology, India

Chair of Advisory Committee Dr. Ying Qi

Near-road air quality studies have indicated the presence of high levels of pollutants. In this study, a three dimensional Eulerian model is developed which can be used to study the air quality near freeways. A vehicle-induced turbulence parameterization is included in the model to estimate better the turbulent diffusion of pollutants. The near-road air quality model is used to study two different cases. In the first case, the model is validated using the data from General Motor's SF_6 dispersion experiment, conducted at Michigan in 1976. Sensitivity of the model to meteorology and traffic-related parameters are studied in detail. In the second case, the spatial distribution of ozone, carbon monoxide, NO_x and 1,3-Butadiene near a simulated 8-lane freeway was studied.

Model simulation for the first case yielded better results than US EPA's CALINE models which were previously used for regulatory purposes. Model performance when analyzed at different wind directions shows an overall good performance. The results also show that the model performs well at surface but slightly over predicts pollutant concentration at higher elevations. The simulation results for second case at different directions of wind and at different boundary conditions for model species, places

emphasis on the importance of the inclusion of the chemical mechanism in the study of near-road air quality.

DEDICATION

I would like to dedicate my work to God and my parents who have encouraged me at all the phases of my life. I would also like to dedicate this work to all my teachers since childhood for their enormous support and love.

ACKNOWLEDGEMENTS

I would like to thank my research advisor, Dr. Qi Ying, for his care and effort put forth in my work. I will always be indebted to him for his encouragement. I am honored to have Dr. Bill Batchelor and Dr. Renyi Zhang on my committee, and I would like to express my gratitude for their support throughout my research and studies.

I also thank the University Transportation Center for Mobility (UTCM) for sponsoring my work.

I would also like to thank the faculty and my friends at Texas A&M University for making my stay at Texas A&M a pleasant one.

Finally, I thank my father, mother, grandparents and my sister for their love and confidence shown in me.

NOMENCLATURE

EPA	Environmental Protection Agency
US	United States
SF_6	Sulphur hexafloride
NO	Nitrous oxide
NO_2	Nitrogen dioxide
NO_x	$NO+NO_2$
OH	Hydroxyl radical
HO_2	Hydroperoxy radical
BUTA	1,3- Butadiene

TABLE OF CONTENTS

Page

CHAPTER Page

LIST OF FIGURES

Page

Page

Page

LIST OF TABLES

Page

CHAPTER I

INTRODUCTION

1.1. Air Pollution Due to Vehicle Emissions

Highway vehicles emit significant amounts of air pollutants into the atmosphere. The pollutants emitted directly from vehicles include carbon monoxide (CO), nitrogen oxides (NOx), volatile organic compounds (VOC), and fine and ultrafine particulate matter (PM). Air quality monitoring studies detected elevated concentrations of these compounds within a short distance from freeways. For example, Grosjean et al. (2001) studied the concentration of carbonyls in a four lane tunnel in Pennsylvania and reported a concentration of 16.44 µg/m3; Murena (2007) analyzed BTEX (benzene, toluene, ethyl benzene and xylene) compounds near a three-lane road in Italy and reported concentrations of 21.6, 318.9,121.2 and 541.5 µg/m3 respectively; Kean et al. (2000) observed concentrations of ammonia and CO2 of about 0.384 and 1081 ppm, respectively, near Caldecott tunnel on highway 24 in Berkeley, CA; Zhu et al. (2002) observed the concentration of black carbon and carbon monoxide in the range of 20.3-24.8 µg/m3 and 1.9-2.6 ppm, respectively, near I-710 at the Los Amigos County Club in California.

Brugge et al. (2007) estimated that about 11% of people live within 100 m of freeway in the United States. Various studies have shown that adverse health effects are associated with traffic-related air pollution. Some of them are discussed below.

This thesis follows the style of *Journal of Environmental Engineering*.

Richmond-Bryant et al. (2009) reported that school children are exposed to high concentrations of $PM_{2.5}$ and Black carbon of 150.5 and 8.4 $\mu g/m^3$ respectively at a street canyon in New York, while Kim et al. (2004) observed a clear relation between respiratory diseases and children attending and living near schools located in busy traffic areas in California.

Gauderman et al. (2007) showed that there was a substantial impact of freeway pollution on lung development in children in the age group of 8-18 years. Findings revealed that the lung deficiencies in children living in the range of 500 m from a freeway are more than the ones living 1200 m away. Finkelstein et al. (2004) studied the relation between the rate advancement period i.e. premature mortality rate in people and their living distance from the freeway. Results showed a rate advancement period of about 2.5 years. Venn et al. (2001) showed that the risk of wheeze in children increased with decreasing distance from a road. Balmes et al. (2009) studied the relation between lung function in asthma-affected adults and traffic exposure, and showed that the exposure to any density of road traffic can play a pivotal role in deterioration of health.

Vehicle exhaust is one of the major contributors of green house gases and thus global climate change. Niemeier et al. (2006) estimated that about 10-20% of present ozone radiative forcing is due to global road traffic emissions. Wade et al. (1994) estimated that about 60-70% of global warming due to vehicles is due to carbon dioxide and it is estimated that 1887.4 million metric tons CO_2 per year in United States is from the transportation sector (USEPA 2009). Figure 1.1 shows the contribution of carbon monoxide from different sectors in United States.

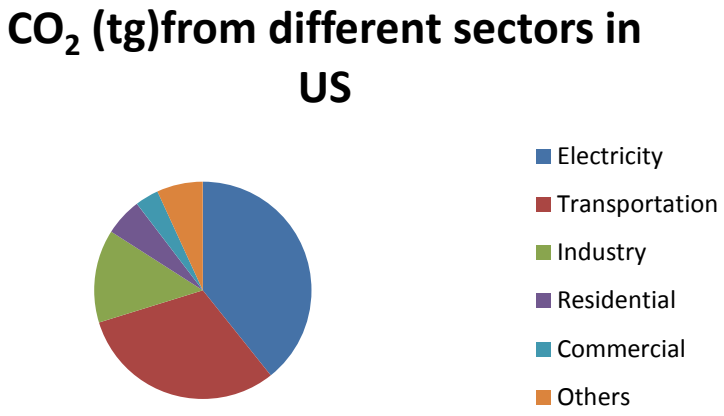

Figure 1.1 Percentage of carbon dioxide emitted from different sectors in US, based on data from US green house gas emission inventory report(USEPA 2009).

1.2. Near-road Dispersion Models

Numerical models are useful tools in understanding the transport and fate of air pollutants near freeways and are often used in exposure studies based on the predicted pollutant concentrations. Models used in near-road studies vary from simple line source models for steady state dispersion of conservative tracers to full-fledged time-dependent grid models with simplified gas phase chemistry. The uniqueness of near-road models to general purpose atmospheric dispersion models is the turbulence caused by vehicle movement.

Sehmel (1973) used zinc sulfide (ZnS) tracer particles to study the re-suspension of particles due to moving traffic. Mass balance on the ZnS tracer particles measured by the downwind samplers showed that the turbulent transport of re-suspended particles depended on vehicular velocity. This vehicle-induced turbulence must be represented appropriately in the models to allow accurate dispersion calculations. Some of the

modeling studies developed to study near-road air quality have been discussed in detail below.

Benson (1992) developed a series of line source dispersion models CALINE3 and CALINE4 based on the Gaussian line source dispersion equation. The highway link was divided into a series of equivalent finite line sources positioned normal to the wind direction. Each element was divided into three sub-elements whose geometry depends on road wind angle. The emission from each element was assumed to be the same. The mixing zone (zone above the freeway where the emissions and the turbulence are assumed to be uniform) was assumed to extend 3 m on either side of the travelled way. In addition to the solar heat flux, which accounts for the stability of atmosphere, an additional heat flux, which is formed due to movement of a vehicle, was used to estimate the stability class in the CALINE4 model. CALINE4 incorporates a simple chemical mechanism to simulate the concentration of reactive NO_2. EPA used CALINE3 and CALINE4 for regulatory purposes before they were replaced by American Meteorological Society and EPA Regulatory Model (AERMOD). This is a Gaussian short range dispersion model developed especially for stationary sources and it can be used for any terrain, but it does not account for vehicle-induced turbulence (Holmes and Morawska 2006).

Held et al. (2003) developed a dispersion model (UCD 2001) in which the highway link is divided into a three-dimensional array of point sources. The concentration of a pollutant at a location is the sum of pollutant dispersed from each of these point sources. A mixing zone, which extended 3 m laterally in each direction and

extended 2.5 m in elevation, was used. SF_6 concentrations near a simulated freeway at a GM testing facility were used to determine the model parameters and to evaluate the model performance. The UCD 2001 model appears to have better performance than the CALINE 4 model.

Kinnee et al. (2004) used a GIS based approach to study the spatial distribution of pollutants from major roads in Houston. The traffic counts data were overlaid on the road layer data in a GIS and interpolated along the length of the road to estimate the traffic flows along the road sections. The US EPA's area source model, ISCST3 was used to evaluate the spatial distribution of benzene along the major roads in Harris County.

Venkatram et al. (2007) conducted a field study adjacent to I-440 in North Carolina to validate the dispersion parameterization used in a line source model developed previously (Venkatram 2004). Traffic related data was collected using a surveillance camera located 5 m from the freeway. Real time NO_x analyzers were located at 20 and 275 m downwind. Wind speed and direction were measured using a two cup anemometer as well as four sonic anemometers located at 5, 20 and 100 m downwind of the freeway. The relation between wind speed and direction measured at sonic anemometers placed at different distances from the freeway showed significant vehicle-induced turbulence. Optical remote sensing instruments were set up parallel to the road at 7 and 17 m downwind of the freeway to study spatial average of NO concentration. The model performed well when the wind was parallel to the freeway but the performance deteriorated as the wind direction changed to oblique.

Sahlodin et al. (2007) used a commercial computational fluid dynamics (CFD) model with moving traffic on a simulated freeway to estimate the vehicle-induced turbulent diffusion coefficients. The vehicle-induced turbulent diffusion coefficients were added to the atmospheric eddy diffusion coefficient to calculate the overall eddy diffusivity for a Gaussian dispersion model. The CFD calculated eddy diffusion coefficients are in general agreement with the values determined by Bäumer et al. (2005).

Rao (2002) developed a two-dimensional grid model called ROADWAY-2 that was based on US EPA's ROADWAY model. The wind, temperature and eddy diffusivity fields were predicted online. The effect of vehicle wake on the turbulent diffusivity was parameterized using vegetation canopy flow theory. The ROADWAY-2 model was validated against the SF_6 data from the GM study. Although a simple chemistry mechanism for O_3 and NO_x was included, no details about the chemistry model and its application were discussed. The ROADWAY-2 model is suitable for studies with a single freeway link but will have difficulty accommodating multiple highway links due to its 2D limitation.

1.3. Objective

Although significant progress has been made in the numerical simulation of near freeway air pollution, much of the effort so far has been focused on pollutant dispersion. Little is known about the formation, destruction and transformation of primary emitted pollutants in the near-road environment, due to lack of complete representation of the chemistry and physics. High concentrations of volatile organic compounds and NO_x in

the near-road environment are expected to produce high concentration of hydroxyl radical and other intermediate free radicals during the day. This could potentially change the chemical composition of the air parcel as it travels downwind. The overall goal of this study is to develop a three-dimensional near-road air quality model with a modern gas phase photochemical mechanism that can be used to study the transport and physical/chemical transformation of gaseous pollutants in areas with multiple freeways links and other sources.

CHAPTER II

DESCRIPTION OF THE NEAR-ROAD CHEMICAL TRANSPORT MODEL

2.1. General Chemical Transport Model Formulation

The reactive transport equation for a species ‘i’ in 3D Cartesian coordinates is given by equation (2.1).

$$\frac{\partial C_i}{\partial t} = -\frac{\partial (UC_i)}{\partial x} - \frac{\partial (VC_i)}{\partial y} - \frac{\partial (WC_i)}{\partial z} + \frac{\partial}{\partial x}\left(K_{xx} \frac{\partial C_i}{\partial x} \right) + \frac{\partial}{\partial y}\left(K_{yy} \frac{\partial C_i}{\partial y} \right) + \frac{\partial}{\partial z}\left(K_{zz} \frac{\partial C_i}{\partial z} \right) + R_i + L_i + S \tag{2.1}$$

where U, V, W indicate wind speed in x, y and z directions respectively; C denotes concentration of species ‘i’, K_{xx}, K_{yy} and K_{zz} are the turbulent diffusivities in x, y and z planes; R and L denote the rate of production and loss due to chemical reactions respectively; and S is the emission rate of the species ‘i’ .

2.1.1. Turbulence parameterization

As observed in section 1.2, even though studies in the vicinity of a roadway indicated that turbulence created by moving traffic plays an important role in the near-road diffusion of the pollutant, very few models explicitly include this additional turbulence created near a freeway. In the present study we used a new parameterization developed by Bäumer (2005) in a three-dimensional chemical transport model. In this parameterization scheme, the overall turbulent diffusivity near a freeway is assumed to

be a linear summation of atmospheric and vehicle–created turbulent diffusivities, as shown in Equation (2.2).

$$K_{jj} = K_{jj,atm} + K_{jj,mw} \tag{2.2}$$

where $K_{jj,atm}$ is eddy diffusivity due to atmospheric turbulence, $K_{jj,mw}$ is the additional eddy diffusivity due to vehicle-induced turbulence, along the axis 'j'. The atmospheric turbulent diffusivity is determined based on the Monin-Obukhov similarity theory (Monin and Obukhv 1954; Stull 1988). The parameterization scheme used in this study is summarized in Jacobson (2005) and is briefly described below.

The $K_{jj,atm}$ in the surface layer of the atmospheric boundary layer is calculated using Equation (2.3).

$$K_{atm} = \frac{\kappa u_* z}{\phi(z/L)} \tag{2.3}$$

where z is the height at which the atmospheric diffusivity is calculated, u_* is the calculated surface friction velocity. Von Karman constant (κ) is taken as 0.35. Parameter ϕ is used to account for the stability of the atmosphere and is calculated based on the Monin-Obukhov length (L), which in turn is calculated using Equation (2.4).

$$L = \frac{u_*^2 t_s}{\kappa g t_*} \tag{2.4}$$

$$t_* = \frac{\kappa(t_s(z_r) - t_s(z_{0,h}))}{\int_{z_{0,h}}^{z_r} \phi(z/L)\frac{dz}{z}} \tag{2.5}$$

where t_* and t_s are potential temperature scale at surface layer and virtual temperature at the ground surface respectively.

Equations (2.6), (2.7) and (2.8) are used to calculate the function ϕ in stable (L>0), unstable atmospheric conditions (L<0) and neutral (L=0) respectively.

$$\phi\left(\frac{z}{L}\right) = 0.74 + 4.7z/L \tag{2.6}$$

$$\phi\left(\frac{z}{L}\right) = 0.74 + (1 - 9 \times z/L) \tag{2.7}$$

$$\phi\left(\frac{z}{L}\right) = 0.74 \tag{2.8}$$

The $K_{jj,mw}$ needs to be evaluated before equation (2.1) can be used to solve the reactive transport of pollutants. Baumer *et al* (2005) suggested to use equation (2.9) for the additional turbulent kinetic energy(e_m) caused by the moving vehicles.

$$\frac{\partial e_m}{\partial t} = -\frac{\partial (Ue_m)}{\partial x} - \frac{\partial (Ve_m)}{\partial y} - \frac{\partial (We_m)}{\partial z} + \frac{\partial}{\partial x}\left(K_{xx}\frac{\partial e_m}{\partial x}\right) + \frac{\partial}{\partial y}\left(K_{yy}\frac{\partial e_m}{\partial y}\right) + \frac{\partial}{\partial z}\left(K_{zz}\frac{\partial e_m}{\partial z}\right) + P - \varepsilon \quad (2.9)$$

In this equation, P and ε denote the rate of production and dissipation of kinetic energy respectively and K_{xx}, K_{yy} and K_{zz} are turbulent diffusivities in the x, y and z directions.

The ability of vehicles to produce turbulence in the atmosphere is a function of their geometries and speeds. Detailed calculation of the vehicle-induced turbulence for every possible vehicle shape and speed combination is too complex to be implemented in a 3D air quality model and has to be parameterized. In the parameterization scheme, the vehicle fleet was divided into two general classes, passenger cars (pc) and heavy duty vehicles (hd). The vehicles are represented by a representative height and width. The production of turbulent kinetic energy due to passenger cars and heavy duty vehicles was calculated using Equation (2.10).

$$P = \frac{0.5}{L_x L_z}\left(c_{d,pc} W_{pc} H_{pc} T_{pc} V_{pc}^2 + c_{d,hd} W_{hd} H_{hd} T_{hd} V_{hd}^2\right) \quad (2.10)$$

here L and c_d denote the grid length and drag coefficient respectively. Mean width, mean height, travel velocity and traffic density of a vehicle class are denoted by W, H, V and T respectively.

The energy dissipation at a height z above the surface is calculated using Equation (2.11).

$$\varepsilon = c_1 \frac{e_m^{1.5}}{z} \tag{2.11}$$

The kinetic energy updated at each time step is used to calculate the coefficient of diffusion due to turbulence created by moving vehicle using Equation (2.12).

$$K_{jj,mw} = \overline{L}_j \times e_m^{0.5} \tag{2.12}$$

where $\overline{L}_j$, the length of a vehicle along an axis 'j' and can be calculated by Equations (2.13) and (2.14).

$$L_{xx} = \left(\frac{T_{pc} W_{pc} + T_{hd} W_{hd}}{T_{pc} + T_{hd}} \right) \tag{2.13}$$

$$L_{yy} = \left(\frac{T_{pc} H_{pc} + T_{hd} H_{hd}}{T_{pc} + T_{hd}} \right) \tag{2.14}$$

2.1.2. Gas phase chemical mechanism

A modified version of the SAPRC99 (Carter 2000) photochemical mechanism was used to perform gas phase chemistry in the near-road environment. SAPRC99 is a lumped chemical mechanism used to study the photo-oxidation of organic compounds and inorganic compounds in the atmosphere and is widely used in regional air quality models. The original version was modified to explicitly include chemical reactions of

some air toxics for vehicular emissions. An asymptotic technique presented in Young and Boris (1977) was used to solve the ODEs of chemical reactions involving sixty nine chemical species included in the model. A list of species is included in Appendix B.

2.2. Solution Techniques for the Reactive Transport Equation

2.2.1. Operator splitting solution of the governing equation

The solution of the reactive transport equation follows the operator splitting procedure described by McRae et al.(1982). In this technique, different parts of the reactive transport equation are solved sequentially using the most suitable technique. For each operator splitting time step Δt, the advective and diffusive transport of pollutants in the horizontal direction is solved using a time step of $\Delta t/2$. The 2D transport is performed by solving 1D transport equation in the x and y individually. In the first $\Delta t/2$ time step, pollutant transport of species in the x direction is followed by the transport in the y direction After the horizontal transport, chemistry, emission, vertical diffusion and dry deposition processes are solved together with a time step of Δt, followed by another horizontal transport calculation with a time step of $\Delta t/2$, with y direction first then x direction, to complete an entire time step of the simulation. In the present study the operating time step was one second. This choice was based on the wind speed in the domain and allows for a stable solution of the transport equation.

2.2.2. Diffusion

The Crank-Nicholson method as shown in Equation (2.15), is used to solve the diffusion of pollutants.

$$\frac{c_i^{n+1}-c_i^n}{\Delta t}=\frac{K}{2x^2}\left(\left[c_{i+1}^n-2c_i^n+c_{i-1}^n\right]+\left[c_{i+1}^{n+1}-2c_i^{n+1}+c_{i-1}^{n+1}\right]\right) \quad (2.15)$$

where n, x and i denote the time step, grid length and grid number respectively. Equation (2.15) can be arranged in the form of a tri-diagonal matrix and was solved using a subroutine from the Numerical Recipe book (Press W.H 1992).

2.2.3. Advection

The piece-wise parabolic method (PPM) is used to solve the advection equation (Corlella and Woodward 1984). The advantage of the PPM method is to allow non-uniform grid size in the model. In this procedure a cubical curve fitting technique which is piece wise continuous in nature is used to interpolate the concentration at each grid edge. The slope of the parabola at the edge of the grid 'j' is given by Equation (2.16).

$$\delta C_j=\frac{\Delta e_j}{\Delta e_{j-1}+\Delta e_j+\Delta e_{j+1}}\left(\frac{2\Delta e_{j-1}+\Delta e_j}{\Delta e_{j-1}+\Delta e_j}\left[C_{j+1}-C_j\right]+\frac{2\Delta e_{j+1}+\Delta e_j}{\Delta e_{j-1}+\Delta e_j}\left[C_j-C_{j-1}\right]\right) \quad (2.16)$$

here Δe_j denotes the size of the grid 'j'.

The concentration at the next time step (C_j^{n+1}) was calculated using Equation (2.17).

$$C_j^{n+1}=C_j+d_j\left(fl_{j-1}-fl_j\right) \quad (2.17)$$

where d_j, a dimensionless number given by Equation (2.18), was plugged into Equation (2.19) to calculate fl_j.

$$x_j = \frac{u_j \Delta t}{e_j} \tag{2.18}$$

$$fl_j = C_{rj} - \left(\frac{x_j}{2} \times \left[\left\{ C_{rj} - C_{lj} \right\} - \left\{ \left[1 - \frac{2x_j}{3} \right] \times C_{6,j} \right\} \right] \right) \tag{2.19}$$

here e, u, C_r and C_l represent size, wind velocity, and concentration at the right and left boundary respectively. $C_{6,j}$ is given by equation (2.20).

$$C_{6,j} = 6(C_j^n - 0.5(C_{rj} + C_{lj})) \tag{2.20}$$

CHAPTER III

MODELING SF_6 DISPERSION NEAR A SIMULATED FREEWAY

3.1. The GM Experiment

General Motors conducted experiments at its Milford Proving Ground in 1976 to study the exposure to sulfate near roadways. The study was done on 17 different days starting from September 27th to October 30th. The experiments were conducted on a simulated 4-lane bidirectional freeway using 352 catalyst equipped cars divided into 32 packs, 16 packs of cars in each direction. The fleet also included eight pickup trucks, equipped with cylinders releasing SF_6 at known rates to study dispersion near freeways. Each pickup truck was placed four packs apart. Figure 3.1 shows a section of the freeway with pack of cars.

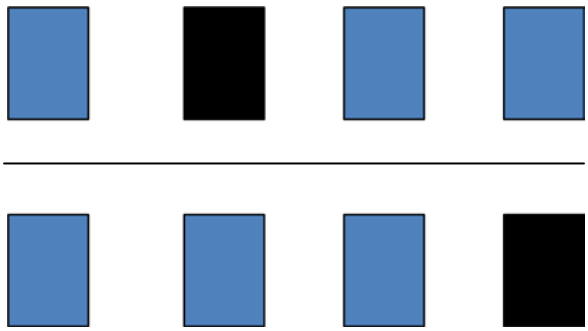

Figure 3.2 A section of the freeway showing pack of cars. A pack of cars with a truck is represented with a different colored pattern.

The meteorological conditions and the concentration of sulfate and SF_6 were measured at six towers arranged in the upwind and downwind locations near the simulated freeway. Wind direction at the GM Proving Ground during the experiment was generally from west to east. Tower 1 and 2 were at 30 m and 2 m west of the freeway left boundary (in the upwind direction), respectively. Tower 3 was placed at the median of the freeway, which separated the north and south bound traffic. Towers 4-6 were arranged at 4, 15 and 30 m east of the freeway right boundary (downwind), respectively. In addition to these towers, two stands were placed at 50 and 100 meters east of the freeway to measure concentrations and meteorological conditions 0.5 and 1.5 meters above the surface, respectively. All the towers and stands were placed in a straight line, as shown in Figure 3.2.

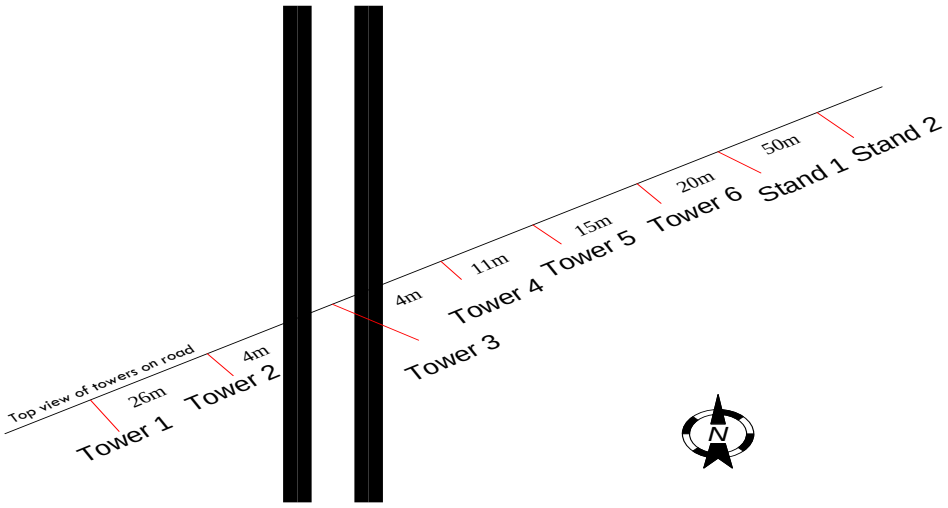

Figure 3.3 The alignment of six towers and two stands that measures the meteorology and pollutant concentrations near the GM test track.

The arrangement of the samplers and meteorological instruments on the towers can be seen in Figure 3.3**.** Temperature was measured at three different heights i.e. at 1.5, 4.5 and 10.5 m on towers 1 and 6. UVW anemometers, used to measure wind speed in x, y and z directions, were placed at three heights i.e. 1.5, 4.5 and 10.5 m on all the towers and at 1.5 m on the two stands. Syringe samplers were placed at 0.5, 3.5 and 9 m above surface to collect SF_6 samples in all the towers and at 1.5 m height on the stands. The collected samples were analyzed using a gas chromatograph to determine the SF_6 concentration.

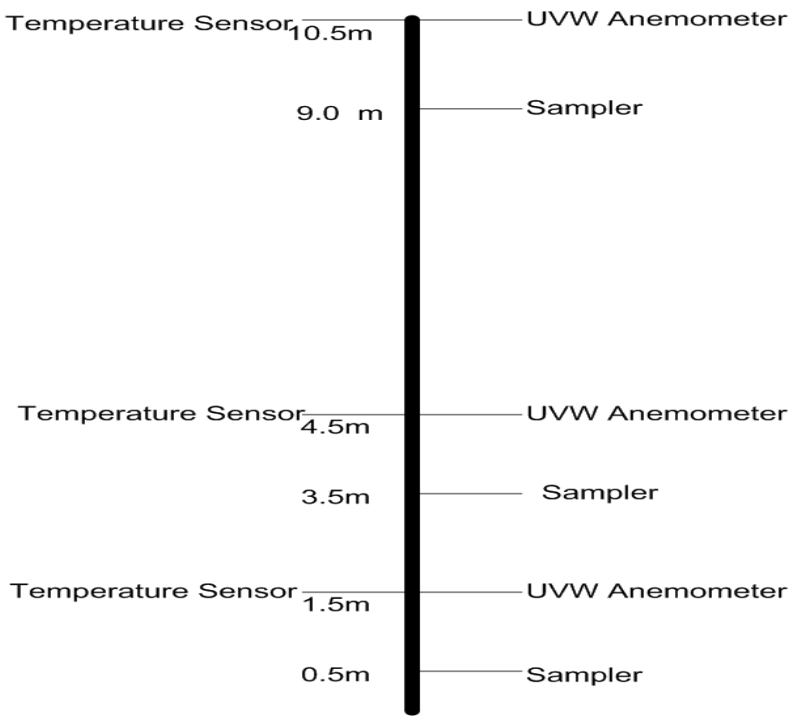

Figure 3.4 Schematic view of a tower showing the position of samplers, anemometers and temperature sensors.

Sampling started at 7:35 AM and ended at 9:35 AM on most of the 17 study days. In this period, four half-hour samples were collected. Each sample was denoted by a specific number 'dddhhmmss' which will be referred hereafter as a "scode". For example, scode 296083459 denotes the half hour sample collected on 296th Julian day of the year, from 8:04:59-8:34:59. A total of 66 SF_6 tracer data were collected during this study. However, not all the samples collected could be used for analysis. On day 272, leaks in the SF_6 tracer release system were observed. On days 272-276, thermometers used to collect temperature data at the 30m west tower (tower 6) malfunctioned. As temperature is used in the calculation of atmospheric diffusivity, we excluded the data collected on these days from our calculations and thus ended up with 50 scodes for analysis.

3.2. Model Domain

The modeling domain in this study is rectangular domain of 600x600 meters in the horizontal direction and 40 meters in the vertical direction. The domain was divided into 100*100*11 grids. Each grid cell is 6x6 meters in the horizontal direction**.** The 4-lane north-south freeway was placed at 42, 48, 66 and 72 meters from the left boundary of our domain. The model domain is shown in Figure 3.4. The vertical spacing of the grid cells varies from 1 m near the surface to 10 meters in the top layer. i.e., the height of each layer is 1m, 1m, 2m, 2m, 2m, 2m, 4m, 4m, 6m, 6m and 10m respectively from bottom. A finer vertical spacing near the surface was taken to study the pollutant transport in detail in the lower regions of atmosphere.

As the meteorology available from the GM experiment was only till a height of 10.5 m above the surface, a logarithmic wind profile was inserted in order to extrapolate the data to higher elevations in the domain.

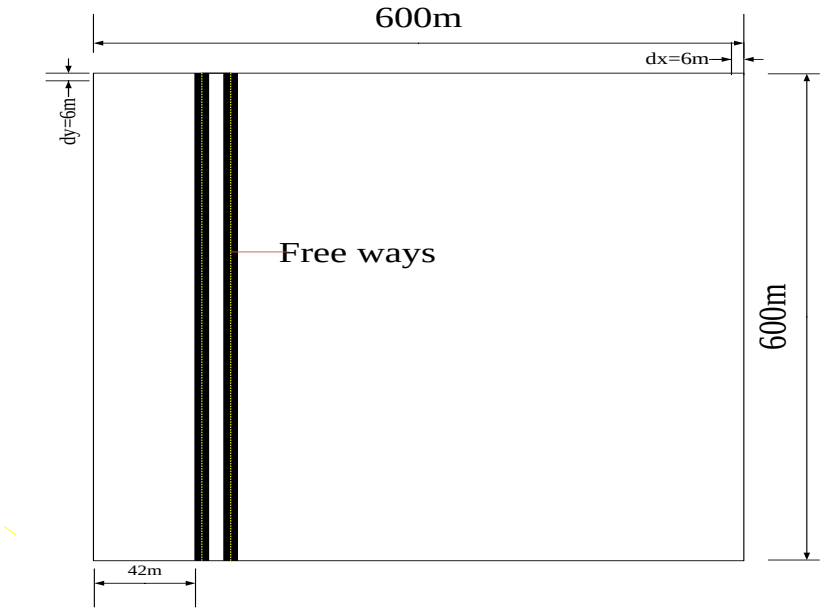

Figure 3.5 Model domain showing the presence of freeway.

3.3. Vehicle Density and Emission Rate of SF_6

The total amount of SF_6 emitted from all the trucks in a lane was averaged over all the grids in that lane, i.e. emission rates of SF_6 in l/min in each lane (f) was converted into ppm/s in each road grid (F) using equation (3.1). Here 8.4e-7 is the conversion factor from l/min from a lane to ppm/sec in a grid. For example, on Julian day 272 the flow

rate was reported as 1.41 l/m from an inside lane, and is calculated as 11.84 e-7 ppm/s per a grid.

$$F = f 8.4 \times 10^{-7} \tag{3.21}$$

The number of vehicles (N) in a freeway grid of area (a) was calculated using the vehicle density per unit area using equation (3.2). The vehicle density was 0.003 vehicles/area, which is about 0.1(0.003*36) vehicles per grid.

$$N = n \times a \tag{3.22}$$

As there no chief sources of SF_6 apart from the amount emitted from the cylinders placed in the trucks, the boundary concentration and the initial concentration of SF_6 are considered as 0.

3.4. Results and Discussion

3.4.1. Determine the parameters of vehicle-induced turbulence

The parameterization used to calculate vehicle-induced turbulent diffusivity had two empirical constants: c_1 in the energy dissipation term (Equation (2.11)) and $c_{d,pc}$ in kinetic energy production term (Equation (2.10)). Proper values of c_1 and $c_{d,pc}$ were determined using regression analysis. Correlation coefficient (R^2), slope (b_1) and ordinate (b_0) of the linear fit equation were determined by fitting a straight line between the predicted (P_i) and observed (O_i) values using the least square linear fit method.

$$P_i = b_1 O_i + b_0 \tag{3.23}$$

Table 3.1 shows the regression coefficients calculated for different values of c_1; while keeping $c_{d,pc}$ constant(0.3). c_1 was varied from 0.04 to 1 and their corresponding values of regression coefficients was calculated.

Table 3.1 Regression coefficients R^2, b_0, b_1 for different values of c_1

c_1	R^2	b_0	b_1
0.04	0.643	-0.06	1.02
0.05	0.645	-0.06	0.98
0.06	0.647	-0.05	0.95
0.1	0.651	-0.02	0.87
0.2	0.66	0.02	0.75
0.6	0.667	0.04	0.68
0.7	0.688	0.08	0.57
0.8	0.692	0.09	0.55
1.0	0.698	0.1	0.53

From Table 3.1, it is observed that the value of R^2 and b_1 are relatively constant when compared to b_0, which decreased with an increase in c_1. The best possible set of R^2, b_0 and b_1 were observed for a c_1 value of 0.1, which happened to be the value suggested in Bäumer et al.(2005) .

Table 3.2 shows the regression coefficients calculated for a range of $c_{d,pc}$; while keeping c_1 constant and equal to 0.1. $c_{d,pc}$ was varied from 0.1 to 0.35.

Table 3.2 Regression coefficients R^2, b_0, b_1 for different values of $c_{d,pc}$

$C_{d,pc}$	R^2	b_1	b_0
0.1	0.651	0.03	0.71
0.2	0.66	0.002	0.81
0.3	0.65	-0.02	0.87
0.35	0.64	-0.03	0.89

From Table 3.2, it is observed that the best possible set of R^2, b_0 and b_1 was found for a $c_{d,pc}$ of 0.3.

3.4.2. Base case simulation results

Figure 3.5 shows the observed and predicted concentrations for all the monitor locations in all the 50 scodes analyzed. The concentrations of SF_6 reported are in units of parts per billion (ppb). The three lines shown on the plot are 2:1, 1:1 and 1:2 respectively from top.

The predictions are generally in good agreement with observations, for high concentrations, but a slight over prediction of low concentrations is observed. These low concentrations are mostly the concentrations reported at the higher levels, as discussed in detail in the next few sections.

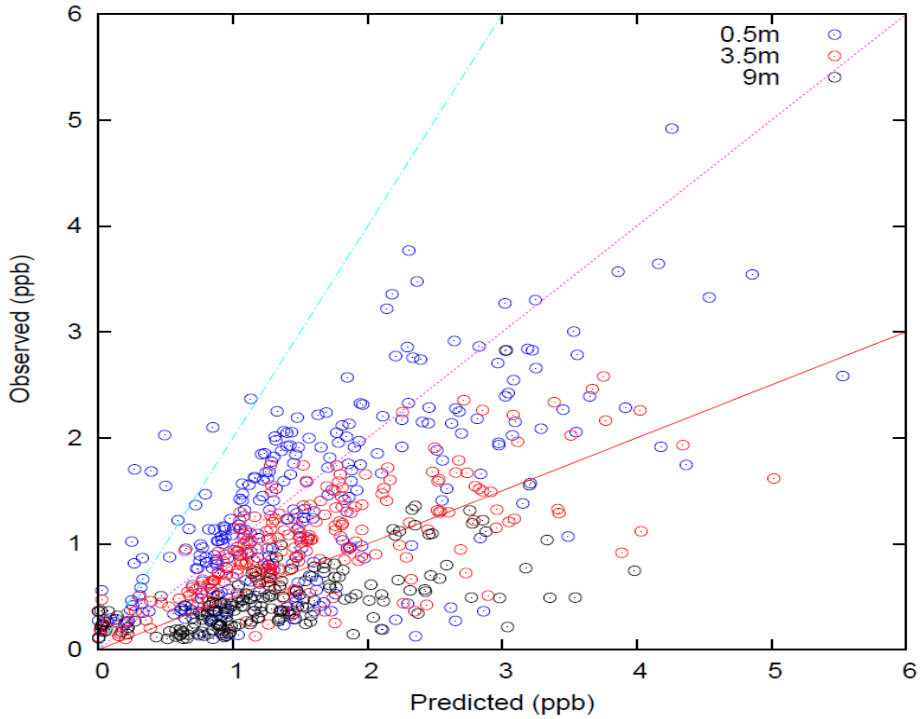

Figure 3.6 Observed and predicted concentrations of SF_6 at all monitor locations for all the cases analyzed.

To study the model performance for different wind directions, the 50 experiments were divided into four categories: 225-315 degrees (perpendicular to the freeway from east to west, category A), 315-337.5 and 202.5-225 degrees (oblique to the freeway, category B), 22.5-157.5 degrees (from east to west, category C), and 337.5-22.5 and 157.5-202.5 degrees (parallel to the freeway, category D). Data from category C is not used in the analysis as most of the sampling towers were in the upwind direction. Normalized mean square error (NMSE) and Fractional bias (FB) given by equations (3.4) and (3.5) respectively, were used as statistical measures for model performance.

$$NMSE = n \times \frac{\sum_{i=1}^{n} (P_i - O_i)^2}{\left(\left[\sum_{i=1}^{n} P_i \right] \times \left[\sum_{i=1}^{n} O_i \right] \right)} \tag{3.24}$$

$$FB = 2 \times \frac{\left(\left[\sum_{i=1}^{n} P_i \right] - \left[\sum_{i=1}^{n} O_i \right] \right)}{\left(\left[\sum_{i=1}^{n} P_i \right] + \left[\sum_{i=1}^{n} O_i \right] \right)} \tag{3.25}$$

where P_i denotes predicted, O_i represents observed SF_6 concentrations at the i^{th} data point and n denotes the total number of data points considered. As discussed earlier a total of fifty 30-minute samples (scodes) were considered for analysis. Data points having observed concentrations of less than 0.1ppb were neglected in this analysis.

NMSE and FB values for the three wind categories A, B and D are shown in the Table 3.3**.** Lesser NMSE and FB values indicate better performance. A positive FB value indicates over prediction and vice versa. The results of ROADWAY-2 model, adapted from Rao (2002), are also shown in the same table for comparison purposes.

Table 3.3 Fractional Bias (FB), Normalized Mean Square Error (NMSE) for all the data points and three different wind categories. Results of ROADWAY-2 model (Rao 2002) are also shown

Wind Category	This study			ROADWAY-2 (Rao 2002)		
	FB	NMSE	n	FB	NMSE	n
A	0.1	0.21	148	-0.11	0.3	56
B	0.31	0.27	117	-0.55	0.52	55
D	0.53	0.69	353	0.12	0.1	56
ALL	0.4	0.52	700	-0.18	0.29	167

FB and NMSE for cases where wind is perpendicular and oblique to the freeway yielded better results in this study when compared to the ROADWAY-2 model.

Reported FB and NMSE values of ROADWAY-2 are slightly better than our model results (i.e. FB of 0.53; and NMSE of 0.69) for Category D, wind blowing parallel to freeway. A smaller selected sample range (n) considered by the ROADWAY-2 for analysis may be one of the reasons for its better performance.

FB and NMSE values for all the data points irrespective of their wind categories are 0.4 and 0.52 respectively. The difference in overall performance of these two models can be due to non-inclusion of data which fall under Category C and a relatively smaller data set used in ROADWAY-2 analysis.

Sum of Squared Residuals (SSR) and α, which denotes the percentage by which the predictions vary with observations, were calculated for the complete data set using equation (3.6) and (3.7), respectively and they are shown in the Table 3.4**.** According to Rao et al. (1986) a α value of 30 shows excellent model performance. Held et al. (2003) used the same GM data to analyze his model (UCD 2001) and US EPA's previously used regulatory models CALINE3 and CALINE4. These evaluation results, adapted for comparison purpose in this study, are also presented in the table below.

$$SSR = \sum_{i=1}^{n} \left(P_i - O_i \right)^2 \tag{3.26}$$

$$\alpha = \sqrt{\frac{SSR}{\sum_{i=1}^{n} P_i^2}} \tag{3.27}$$

Table 3.4 α and SSR for our model, UCD 2001, CALINE3 and CALINE4 for all the scodes analyzed (N_s).Note Results for UCD 2001 and CALINE models were adapted from (Held et al. 2003)

Model	α (in percent)	SSR	N_s
This study	50	544	50
UCD 2001	38	180	62
CALINE3	104	1353	62
CALINE4	92	1068	62

These results indicate that performance of our model is comparable to UCD2001, while it is better than CALINE3 and CALINE4 models. As discussed earlier, a total of twelve scodes which had a problem with measured temperature were not analyzed by our model. The other models reported in table above, are less temperature dependent and so may have included those 12 scodes in their analysis.

3.4.3. Effect of vehicle-induced turbulence

Figure 3.6 depicts the importance of vehicle-created turbulence in the model. The observed and predicted concentrations for all fifty scodes analyzed for two different cases, one case including vehicle-induced turbulence; and the later without vehicle-induced turbulence, are shown.

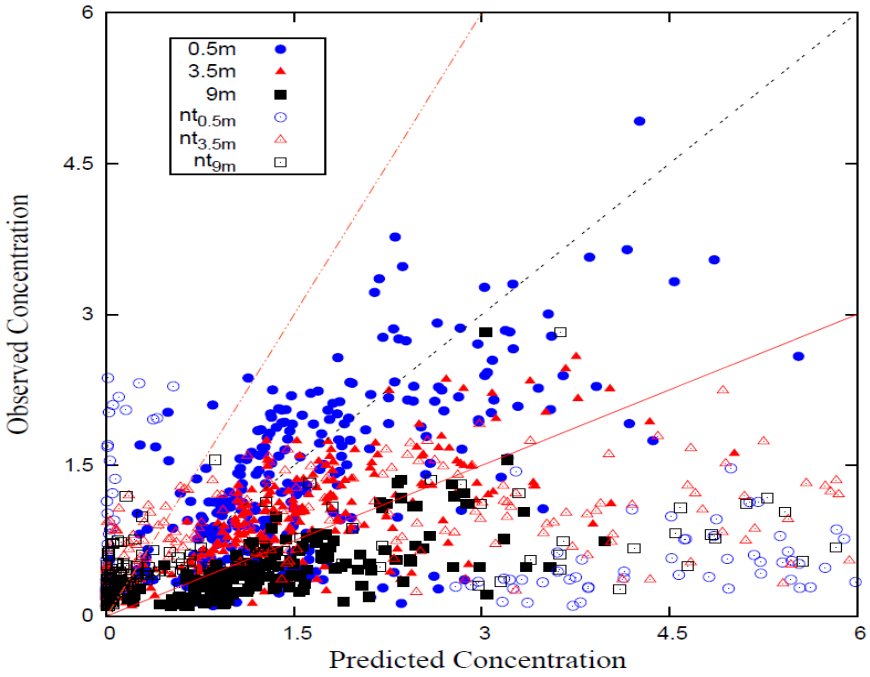

Figure 3.7 Observed and predicted concentrations for all scodes analyzed, for the base case and the case without vehicle-induced turbulence. The three lines shown in the plot indicate observed to predicted ratio of 1:2, 1:1 and 2:1.

The performance of the model, as shown in the Figure 3.6, is better for the case where vehicle-induced turbulence is included. The figure helps in understanding the relative performance of these two cases at different heights. From figure we observe that the most of the predictions at lower layers resulted in overprediction but the predictions at higher layers lead to a underpredction when the vehicle-created turbulence is not included in model mechanism. As in the case where vehicle-created turbulence is not included in the model, the diffusion of SF_6 to higher layers from the surface layers due to the additional turbulence created by the moving vehicles is absent. This leads to an overprediction of surface layer concentrations and an underprediction at higher layers.

3.4.4. Concentration as a function of distance

Figure 3.7 shows the change in averaged observed and predicted concentrations with distance at three different heights (0.5, 3.5 and 9 m) above the surface for three different wind categories (A, B and D). Error bars are used to represent the standard deviation of each data point.

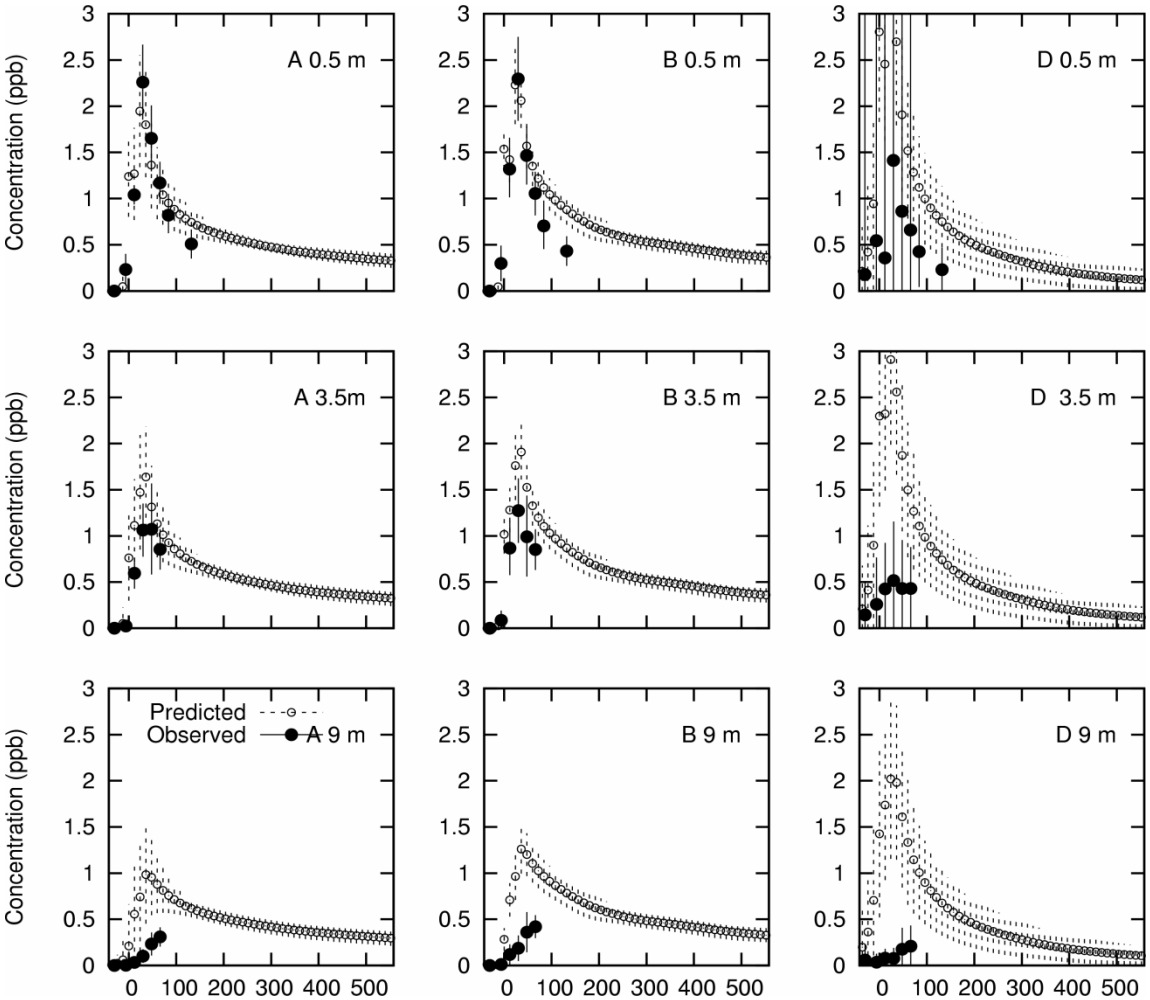

Figure 3.8 Mean and standard deviation of all observed and modeled concentrations of data points collected at 0.5, 3.5 and 9 m above the surface for wind categories A, B and D. Error bars represent standard deviations.

A significant rise in concentration occurs at 40 to 70 m from the left boundary, which is caused by the presence of the freeway. The predictions are in good agreement with the observations for surface layer (0.5m) and the layer above the surface (3.5m). A slight over-prediction of lower concentrations is observed, especially at a height of 9m.

3.4.5. Concentration as a function of height

Figure 3.8 shows the vertical profiles for averaged observed and predicted concentrations at tower 3, 4 and 5, located downwind of the freeway. The plots for three different categories A, B and D are shown in the three panels. Error bars represent standard deviation.

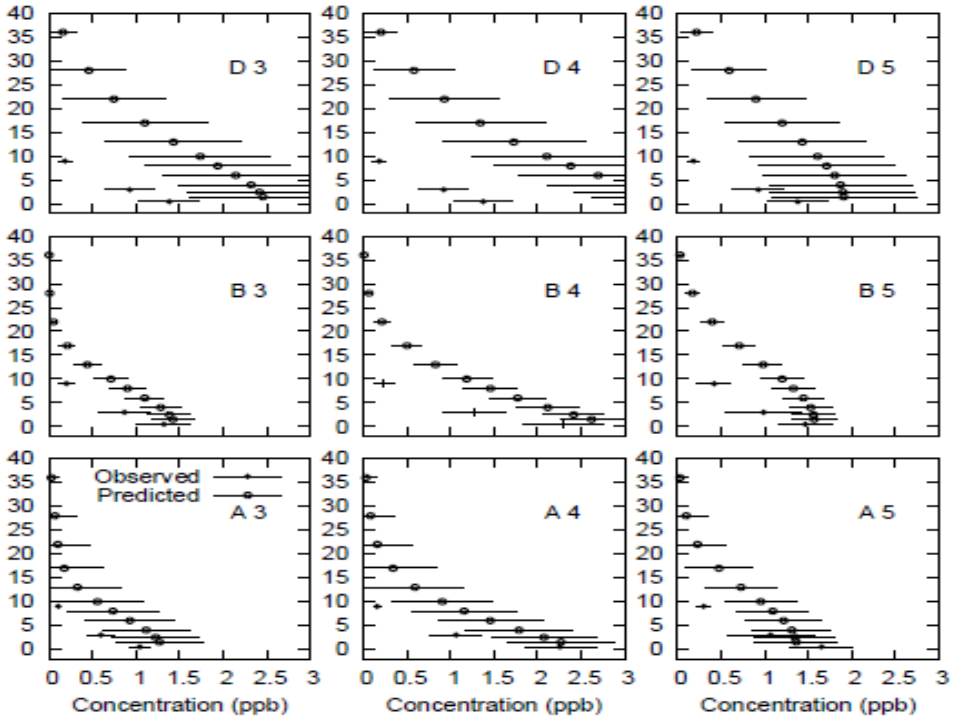

Figure 3.9 Mean observed and predicted concentrations of all data points for three wind categories A, B and D at downwind towers 3, 4 and 5 shown in Figure 3.3.

A clear fall in concentrations with an increase in height is observed in Figure 3.8, illustrating the fact that higher concentrations are observed at the surface levels, where it is released. The model performance is good for all the wind categories at surface layers but a slight overprediction of concentrations is observed at higher layers. As discussed in the previous chapter, a logarithmic wind profile formed by using the observed wind at lower layers is used to extrapolate the wind speed at higher layers. This extrapolation might have lead to an inaccurate wind field at higher layers affecting the diffusivity at that layer. An erroneous diffusivity might have affected the mass transfer in horizontal and vertical directions in that domain.

3.4.6. Sensitivity studies

Sensitivity of model to meteorology and vehicle-related parameters used in the model was studied in detail. Figure 3.9 and Figure 3.10 depict the importance of vehicle parameters and their role in vehicle-created turbulence. Figure 3.11 shows the sensitivity of the model to uncertainties in observed meteorology.

Figure 3.9 shows the sensitivity of the model to vehicle speed, when the number of vehicles and the total emission from each lane is kept constant. This is designed to test the effect of the vehicle speed on the predicted vehicle-induced turbulence and its effect on the pollutant concentration. The results of predicted concentrations for two cases, i.e. a case where the vehicle speed was doubled another in which the vehicle speed was halved and the base case is shown.

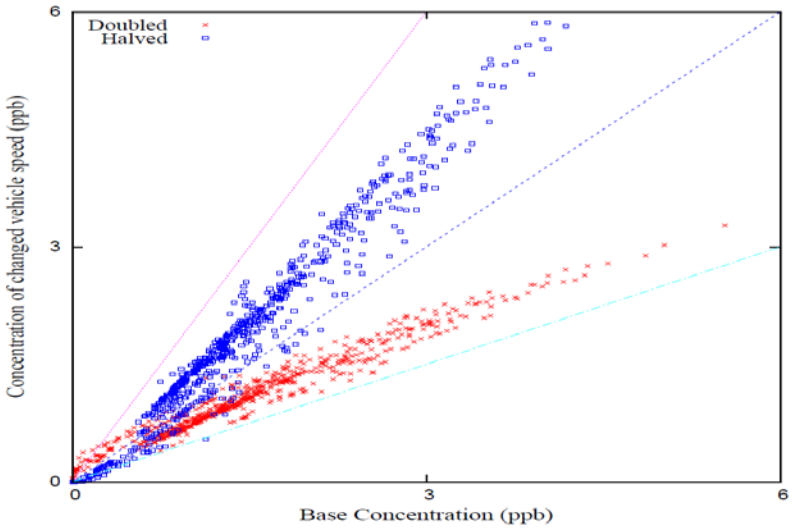

Figure 3.10 Predicted (surface) concentrations for two modeled cases, varying vehicle speed; and the base case; for all the scodes analyzed. The line indicates ratio of base case concentrations to concentration with changed vehicle speed equal to 1.

From the Figure 3.9 an increase in surface layer concentrations with a decrease in vehicle speed and a decrease in surface concentrations with an increase in vehicle speed is observed. As the total amount of emissions from the freeways is constant, this increase is mainly due to the velocity term used in the calculation of production of kinetic energy, i.e. in Equation (2.10). Higher vehicle speeds lead to higher vehicle-created turbulence which in-turn results in more transfer of concentrations from surface layers to higher layers. Similarly, smaller vehicle speeds lead to less transfer of surface concentrations resulting in lesser concentrations at higher layers.

Figure 3.10 shows the sensitivity of model to vehicle density when the total emission and vehicle speed are kept constant. The results of predicted concentrations for two cases, vehicle density halved in one and doubled in another; with respect to their respective base case concentrations are shown.

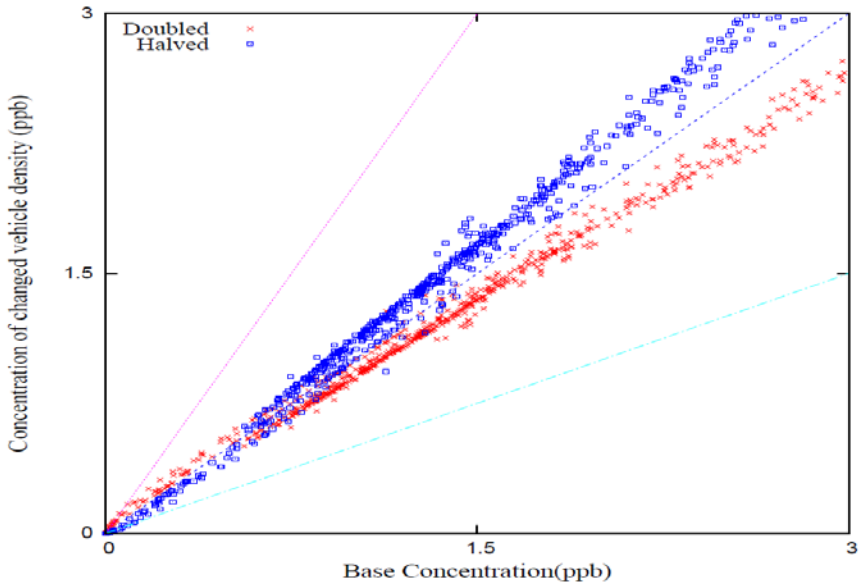

Figure 3.11 Predicted concentrations of two modeled cases, obtained by varying vehicle density; and the base case; for all the scodes analyzed. The line indicates ratio of base case concentrations to concentration with changed vehicle density, of 1.

In the Figure 3.10, we observe a trend similar to Figure 3.9. The more intense change in Figure 3.9 is due to the use of squared vehicle speed in equation (2.10). As the total emission from a lane is maintained constant, higher vehicle density lead to higher transfer of mass from surface layers to higher layers, resulting in a fall in concentration ranges observed at surface layers.

Monte Carlo simulations were used to study the sensitivity of the model to possible discrepancies in observed wind speed and calculated diffusivity. A total of 100 simulations were conducted with varying wind speed and atmospheric diffusivity for each scode. For each simulation, a new set of wind speed and atmospheric diffusivity was generated based on a Gaussian distribution curve. We assumed that wind speed and diffusivity follow a normal distribution with a standard deviation of 30%. To make the figure more readable we included only four representative scodes in Figure 3.11, each represents a different wind category Figure 3.11 shows the mean of all predicted concentrations, calculated by averaging the concentrations and their corresponding observations. An error approximately equal to 10% was reported to be present in the observed concentrations in the GM report (Cadle et al. 1976) and is shown as error bars in the figure.

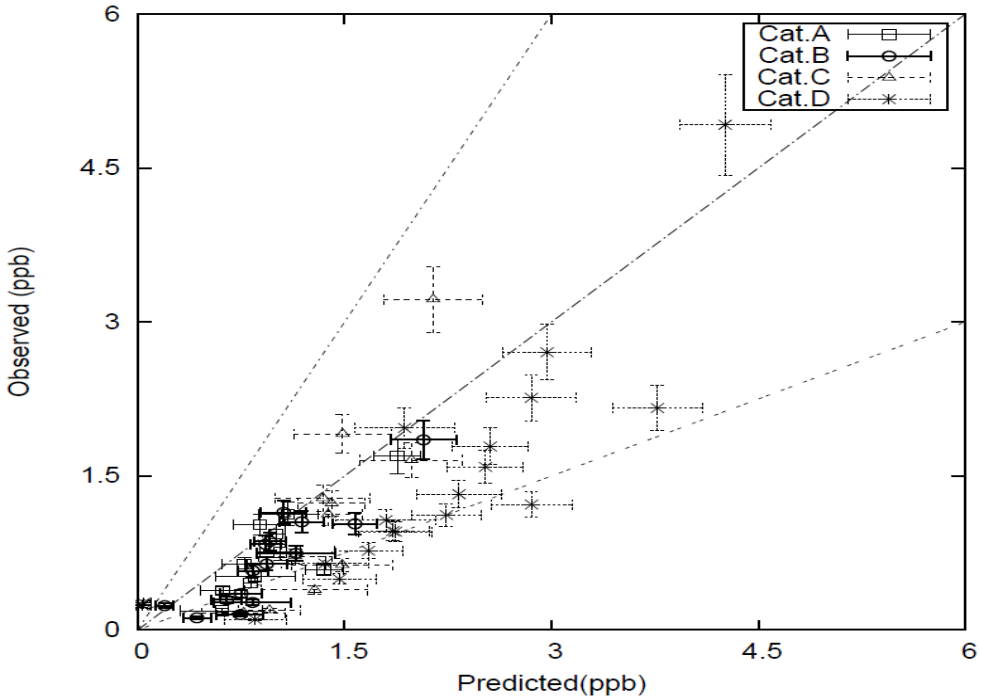

Figure 3.12 Predicted concentration of four sample scodes, falling in different wind categories, whose wind speed and diffusivity were varied by 30%. Averaged values of those predictions with error bars representing standard deviations are presented.

From Figure 3.11, it is observed that the performance of the model is good in all the wind categories. This indicates that a possible discrepancy in the observed wind and calculated diffusivity is not going to alter the performance of the model significantly.

CHAPTER IV

GAS PHASE CHEMISTRY SIMULATIONS

4.1. Introduction

A unique feature of the model developed in this study is that it incorporates the SAPRC99 gas phase atmospheric chemistry mechanism Carter (Carter 2000) that can be used to predict the formation and transformation of reactive air pollutants in a near-road environment. A detailed list of SAPRC99 species is included in the Appendix B. As reviewed in Chapter I, most near-road air quality models are dispersion models and do not have a chemistry module. This limits their application in predicting only non-reactive chemical species. In this section, the importance of incorporated chemistry is studied in detail.

The important chemical reactions, which help in better interpretation of the results, are adapted from Seinfeld and Pandis (2006) and listed below (R4.1-R4.12).

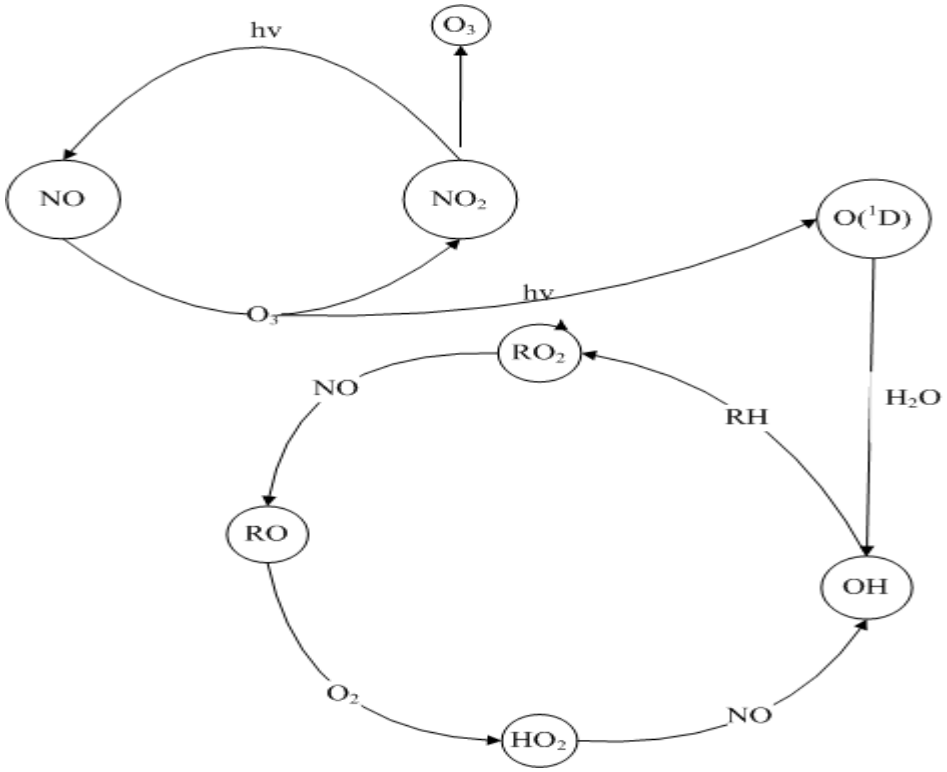

Figure 4.1 Basic day time photochemical reaction cycle of NO, NO_2, radicals and ozone in troposphere.

$$NO_2 + h\nu \rightarrow NO + O$$ R4.1

$$O + O_2 + M \rightarrow O_3 + M$$ R4.2

$$O_3 + NO \rightarrow NO_2 + O_2$$ R4.3

$$O_3 + h\nu \rightarrow O_2 + O\left(^1D\right)$$ R4.4

$$O(^1D) + H_2O \rightarrow 2OH^{\cdot} \quad \text{R4.5}$$

$$RH + OH^{\cdot} \xrightarrow{O_2} RO_2^{\cdot} + H_2O \quad \text{R4.6}$$

$$RO_2^{\cdot} + NO \rightarrow NO_2 + RO^{\cdot} \quad \text{R4.7}$$

$$RO^{\cdot} + O_2 \rightarrow R'O_2^{\cdot} + HO_2^{\cdot} \quad \text{R4.8}$$

$$HO_2^{\cdot} + NO \rightarrow NO_2 + OH^{\cdot} \quad \text{R4.9}$$

$$HO^{\cdot} + HO^{\cdot} \rightarrow H_2O + O_2 \quad \text{R4.10}$$

$$HO^{\cdot} + HO_2^{\cdot} \rightarrow H_2O + O \quad \text{R4.11}$$

$$HO_2^{\cdot} + HO_2^{\cdot} \rightarrow H_2O_2 + O_2 \quad \text{R4.12}$$

The emissions of NO_x and VOC from diesel and gasoline powered vehicles differ significantly. To better represent a busy freeway with both passenger and commercial traffic, it is necessary to use a reasonable split of gasoline and diesel vehicles in the fleet. Field studies conducted near freeways reported that diesel-powered vehicles represent about 20-30% of the total vehicle fleet (Ntziachristos et al. 2007; Zhu et al. 2002). The

vehicle fleet in the base case of the present study is assumed to consist of 30% diesel and 70% gasoline-powered engines.

To understand the effect of gas phase chemistry on the spatial distribution of air pollutants near freeways, eight different simulations were conducted. The base case simulation replicates a mid afternoon scenario with a constant wind field blowing perpendicular to the freeway, selected from the GM study. The wind speed is approximately 1.3 m/s at 9.5 m above surface and the temperature is approximately 32°C. The upwind concentrations of pollutants are taken from a grid cell near downtown Houston using a regional air quality model simulation. The ozone concentration in the grid cell at noon time is quite low, approximately 30 ppb. This low concentration of ozone is likely due to the titration reaction of ozone with the large amount of NO_x in urban area. A different boundary condition is used in one of the case studies that represent a grid cell in an ozone rich plume downwind of the urban emission area. A complete list of the case studies can be found in table on page 46. A list of boundary species and their concentrations for the high ozone and low ozone scenarios are listed in the Table 4.1.

Table 4.1 Concentration of boundary species for Case 1 (base case) and Case 5 (with high ozone boundary condition)

Species	Case 5	Case 1	Species	Case 5	Case 1
NO2	3.791099	35.12449	TBU_O	1.04E-08	3.34E-09
NO	0.332056	25.22054	ACET	2.869435	0.8624
O3P	1.54E-06	4.16E-06	NPHE	5.85E-02	2.57E-02
O3	141.2446	21.99543	PHEN	1.03E-03	3.64E-02
NO3	1.33E-03	4.91E-05	BZNO2_O	2.06E-06	3.61E-09
N2O5	1.04E-03	5.17E-04	HOCOO	4.02E-06	6.16E-09
HNO3	7.459017	4.299823	HCOOH	0.958399	9.38E-02
O1D2	6.90E-12	1.05E-12	RCHO	2.877141	1.005137
HO	5.30E-04	8.05E-05	GLY	0.162339	5.95E-02
HONO	1.75E-02	0.198843	MGLY	0.463394	9.37E-02
HO2	5.69E-02	2.69E-04	BACL	3.44E-02	1.17E-02
CO	210.6542	627.6038	CRES	1.26E-02	5.08E-02
HNO4	3.52E-02	1.93E-03	BALD	2.69E-02	4.43E-02
HO2H	2.077348	8.26E-02	METHACRO	0.210254	0.13192
SO2	17.12872	16.63903	MVK	0.648773	0.132364
SULF	1.13E-02	2.88E-03	ISOPROD	0.110603	8.80E-02
C_O2	2.02E-02	3.78E-05	DCB1	5.03E-02	0.12693
HCHO	10.9278	3.090503	DCB2	4.20E-03	6.39E-03
COOH	0.465848	5.70E-02	DCB3	1.36E-03	1.88E-03
MEOH	2.854117	1.097395	ETHENE	1.245501	4.387082
RO2_R	1.95E-02	1.01E-04	ISOPRENE	0.108218	0.123703
ROOH	1.537259	5.73E-02	TRP1	1.39E-03	2.59E-02
R2O2	4.78E-03	2.98E-05	ALK1	1.197291	2.992554
RO2_N	1.29E-03	9.53E-06	ALK2	1.209846	2.859279
RNO3	1.805857	0.487815	ALK3	2.836475	5.161239
MEK	3.317068	0.361934	ALK4	0.916839	4.732314
PROD2	1.803908	0.492026	ALK5	0.397094	3.25075
CCO_O2	6.28E-03	8.94E-06	ARO1	0.315296	2.007579
PAN	3.382097	7.52E-02	ARO2	0.125331	1.109794
CCO_OOH	0.417676	1.06E-02	OLE1	0.109478	1.544092
CCO_OH	0.797944	0.10623	OLE2	3.16E-02	0.734916
RCO_O2	2.75E-03	2.97E-06	PBZN	1.60E-02	1.38E-03
PAN2	2.150446	3.81E-02	BZ_O	3.06E-06	1.17E-07
CCHO	4.7612	1.506851	MA_RCO3	4.18E-04	6.29E-07
RCO_OOH	0.238483	3.92E-03	MA_PAN	0.420335	1.03E-02
RCO_OH	1.556649	0.141431	BZCO_O2	1.42E-05	7.84E-08

The major differences in the two cases are the abundance of primary emitted compounds. For example, the family of lumped alkanes, aromatics and olefins, is present at high levels in Case 1 and a higher concentration of photochemical oxidation products such as PAN (Peroxy Acetyl Nitrate) are present in Case 5. This indicates that Case1 represents a region in an urban area with fresh emissions and Case 5 depicts an area farther from the urban area where higher concentrations of products are observed.

4.2. Modeling Emissions from Vehicles

The emission rates of gas phase pollutants from eight different vehicle types were prepared using MOBILE6, the EPA's mobile source vehicle emission factor model. An example run script for the MOBILE6 showing the details of the input parameters used is listed in the Appendix C. MOBILE6 predicts the emission rates of NO_x, CO, VOC and six air toxics namely Benzene (BENZ), Methyl Tertiary Butyl Ether (MTBE), 1,3-Butadiene (BUTA), Formaldehyde (HCHO), Acetaldehyde (ACET) and Acrolein (ACRO), in g/mile for 27 different vehicle types. The air quality model requires emissions in g/s for each grid cell and the photochemical mechanism requires the predicted total VOC concentrations be split into detailed VOC species. The air toxics are also explicitly tracked in the photochemical mechanism.

The Emission factor (EF) in each grid is calculated using equation (4.13).

$$EF = EM.(VS/3600) \tag{4.13}$$

where EF is emission factor of a species in g/s at a freeway grid, EM is the raw emission factor in g/mile, VS is average travel speed of all vehicle types considered in mile/hr.

Emissions of the 27 different vehicle types predicted by the MOBILE6 are lumped into eight more general vehicle types. Table 4.2 shows the emission factors of different species in g/s, for eight different vehicle types, light duty gasoline (LDG), heavy duty gasoline (HDG), motorcycle (MC), light duty diesel truck (LDD), heavy duty diesel vehicle (HDD), gasoline bus (GB), diesel commercial bus (DCB) and diesel school bus (DSB). Although only two vehicle types are used to split the vehicle fleet in our current study, this higher resolution of vehicle types allows the model to be applied to scenarios when detailed vehicle fleet information is available.

Table 4.2 Emission factors (g/s) of different model species for different vehicle types for a vehicle velocity of 60 m/hr

Species	LDG	HDG	MC	LDD	HDD	GB	DCB	DSB
NO	3.98E-04	4.90E-04	2.35E-03	1.00E-03	1.25E-03	8.77E-03	3.56E-04	6.91E-03
NO2	2.09E-05	2.58E-05	1.24E-04	5.28E-05	6.56E-05	4.61E-04	1.87E-05	3.64E-04
CO	1.26E-02	1.54E-02	3.51E-02	4.80E-04	6.09E-04	2.53E-03	1.18E-02	2.43E-02
SO2	1.80E-05	2.49E-05	4.74E-05	2.41E-05	3.36E-05	8.33E-05	8.57E-06	1.01E-04
NH3	9.67E-05	8.57E-05	4.42E-05	6.67E-06	6.67E-06	2.65E-05	1.11E-05	3.12E-05
BENZ	4.94E-06	6.56E-06	5.87E-06	1.46E-06	2.40E-06	1.64E-06	7.27E-06	5.50E-06
MTBE	2.81E-06	4.25E-06	3.97E-06	0.00E+00	0.00E+00	0.00E+00	5.50E-06	9.18E-06
BUTA	9.49E-07	1.65E-06	2.32E-06	9.47E-07	1.56E-06	1.38E-06	5.63E-06	2.41E-06
FORM	4.40E-06	1.04E-05	2.39E-05	7.31E-06	1.20E-05	3.18E-05	2.75E-05	3.48E-05
ACET	1.54E-06	3.01E-06	4.53E-06	1.59E-06	2.61E-06	7.98E-06	6.63E-06	7.69E-06
ACRO	9.03E-08	1.60E-07	1.40E-06	3.55E-07	5.84E-07	7.62E-07	3.12E-07	1.43E-06
ALK1	5.40E-06	8.85E-06	5.66E-06	0.00E+00	0.00E+00	0.00E+00	1.35E-05	0.00E+00
ALK2	4.81E-06	7.88E-06	2.52E-05	0.00E+00	0.00E+00	0.00E+00	1.21E-05	0.00E+00
ALK3	2.24E-05	3.68E-05	1.10E-04	0.00E+00	0.00E+00	0.00E+00	5.63E-05	0.00E+00
ALK4	2.54E-05	4.17E-05	8.53E-05	0.00E+00	0.00E+00	0.00E+00	6.38E-05	0.00E+00
ALK5	1.33E-05	2.18E-05	1.36E-05	0.00E+00	0.00E+00	0.00E+00	3.34E-05	0.00E+00
ARO1	9.39E-06	1.54E-05	1.32E-05	0.00E+00	0.00E+00	0.00E+00	2.35E-05	0.00E+00
ARO2	1.41E-05	2.30E-05	1.47E-05	0.00E+00	0.00E+00	0.00E+00	3.53E-05	0.00E+00
CCHO	7.37E-07	1.21E-06	0.00E+00	3.75E-06	6.17E-06	8.06E-06	1.85E-06	2.00E-05
CH4	7.24E-05	1.19E-04	3.77E-05	2.05E-05	3.38E-05	4.41E-05	1.82E-04	1.09E-04
ETHENE	1.61E-05	2.64E-05	3.83E-05	3.97E-05	6.53E-05	8.52E-05	4.04E-05	2.11E-04
HCHO	2.86E-06	4.68E-06	0.00E+00	1.63E-05	2.68E-05	3.50E-05	7.17E-06	8.68E-05
IPROD	3.31E-08	5.42E-08	0.00E+00	8.19E-07	1.35E-06	1.76E-06	8.30E-08	4.36E-06
ISOPRENE	1.19E-07	1.95E-07	3.62E-07	0.00E+00	0.00E+00	0.00E+00	2.99E-07	0.00E+00
MACR	1.24E-07	2.03E-07	0.00E+00	0.00E+00	0.00E+00	0.00E+00	3.11E-07	0.00E+00
NR	1.14E-05	1.87E-05	1.55E-05	2.96E-05	4.87E-05	6.35E-05	2.87E-05	1.58E-04
OLE1	5.85E-06	9.59E-06	2.09E-05	0.00E+00	0.00E+00	0.00E+00	1.47E-05	0.00E+00
OLE2	1.11E-05	1.81E-05	2.19E-05	0.00E+00	0.00E+00	0.00E+00	2.78E-05	0.00E+00
RCHO	3.99E-08	6.54E-08	0.00E+00	1.78E-06	2.92E-06	3.81E-06	1.00E-07	9.47E-06

The total emission rate of a species in a grid cell is calculated by equation (4.14).

$$E_i = \sum_{j=1}^{M} EF_{i,j} \cdot N_j \tag{4.14}$$

where 'i' is the species index, 'j' is the vehicle type index, EF is the emission factor for a species predicted by Equation (4.13), M is the number of vehicle types, and N is the vehicle density of vehicle type j in a grid cell, given by equation (4.15).

$$N_j = \left(\frac{V_j}{VS_j} \right) . X_x \tag{4.15}$$

where V_j denote the number of vehicles of type 'j' travelling in a lane per hour, VS_j denote the travel speed of vehicle j in meters/hour and X_x denote the length of the grid at which the vehicle density is calculated.

The speciation profiles used to split the overall VOC into detailed SAPRC-99 VOC species are summarized in Table 4.3. Here PC denote a gasoline driven passenger car, HD-gasoline indicate a gasoline driven heavy duty vehicle and HD-diesel show a diesel driven heavy duty vehicle.

Table 4.3 Speciation of VOCs from diesel and gasoline engine exhaust

Species	PC	HD-gasoline	HD-diesel
ALK1	0.000466	0.000229	0
ALK2	0.000415	0.001022	0
ALK3	0.001936	0.004473	0
ALK4	0.002193	0.003455	0
ALK5	0.001148	0.00055	0
ARO1	0.000809	0.000536	0
ARO2	0.001213	0.000595	0
CCHO	6.36E-05	0	0.000661
CH4	0.006241	0.001527	0.003616
ETHENE	0.00139	0.001551	0.006984
HCHO	0.000246	0	0.002867
IPROD	2.85E-06	0	0.000144
ISOPRENE	1.03E-05	1.47E-05	0
MACR	1.07E-05	0	0
OLE1	0.000505	0.000846	0
OLE2	0.000955	0.000888	0
RCHO	3.44E-06	0	0.000313

4.3. Results

Spatial distribution of ozone, nitrogen oxides, 1,3-Butadiene (used to represent air toxics), carbon monoxide (as a non-reactive tracer), hydroxyl and hydroperoxy radicals are predicted. In all these simulations, vehicle density and speeds were maintained constant. The details of the eight simulations are listed in Table 4.4.

Table 4.4 List of case studies conducted in gas phase simulation

Case	Comments
1	Base Case
2	Similar to Case 1, chemistry disabled
3	Similar to Case 1, with wind parallel to the freeway
4	Similar to Case 1, with parallel wind, chemistry disabled
5	With higher boundary ozone concentrations (approximately 140 ppb)
6	Similar to Case 5, chemistry disabled
7	Similar to Case 1, with higher diesel fraction in vehicle fleet. i.e. 50% gasoline powered and 50% diesel powered vehicles
8	Similar to Case 7, chemistry disabled

In all the simulations other than the cases when wind is parallel to the freeway, it took less than 10 simulated minutes for the model to reach steady state in the entire domain. The change of the ozone concentration as a function of time at 6, 36, and 438 m away from the highway is show in Figure 4.2. From the figure, it can be seen that the time for ozone to reach steady state is 50, 125 and 300 seconds at the three different distances. The parallel cases take longer time to reach steady state because the horizontal dispersion in the direction perpendicular to the freeway is mainly due to turbulent diffusion, which is comparatively slower than advection. This suggests that to better simulate the air quality near the freeway when the wind is near parallel, transient simulation is probably needed. The concentration predicted using steady-state assumption may not correctly reproduce the air quality a few hundred meters away from the freeway.

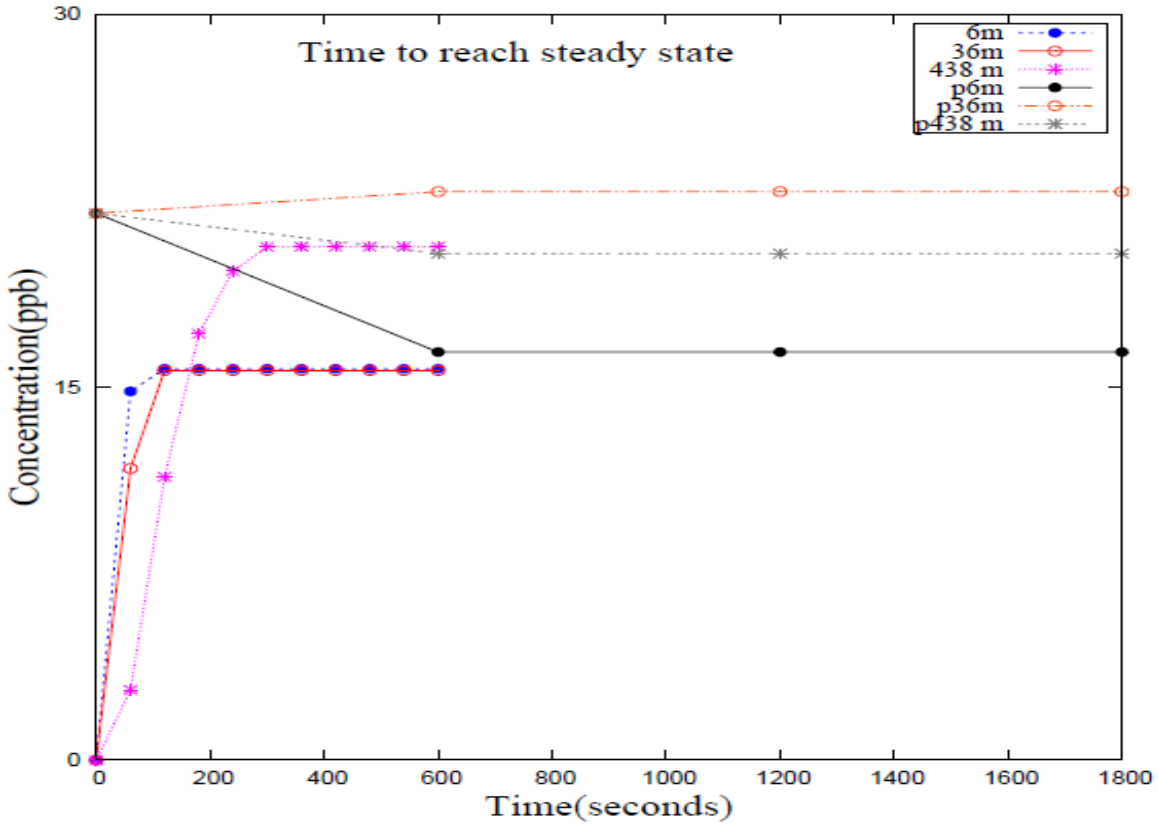

Figure 4.2 Change in ozone concentration with time at 6, 36 and 438 m from the right boundary of the freeway in Case 1(Base case) and Case 3(With wind parallel to freeway and denoted by ‘p’ in the figure).

4.3.1. Base case simulation

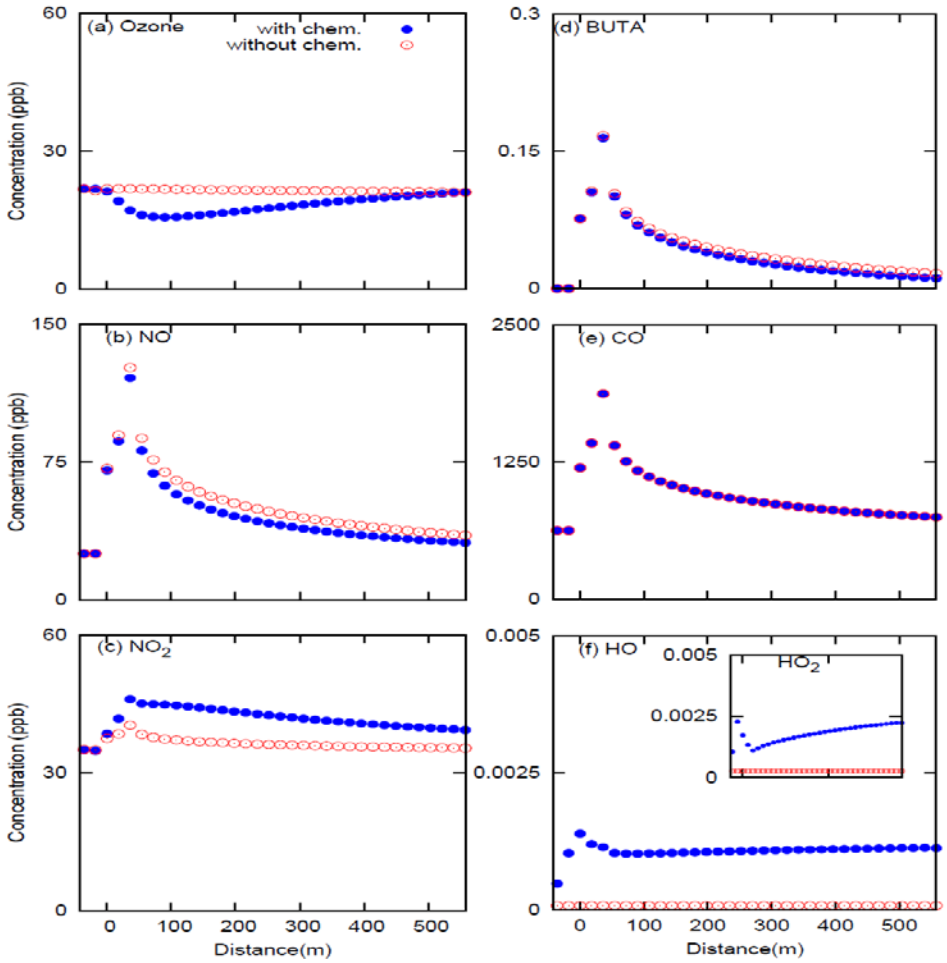

Figure 4.3 Concentration of ozone, nitric oxide (NO), nitrogen dioxide(NO_2), carbon monoxide (CO), 1,3-Butadiene (BUTA), hydroxyl radical (HO) and hydroperoxy radical (HO_2) with and without chemistry at noon time. A positive x-axis indicates downwind distance from the starting point of the freeway.

Figure 4.3 depicts the results of two different simulations, with chemical mechanism included in one (Case 1) and excluded in another (Case 2). From the figure it is clear that there is a slight change in the concentrations of the species due to incorporating chemistry to the model. Changes observed in each of these species are explained below.

A clear decrease in the ozone concentrations near the simulated freeway is predicted when the gas phase chemistry is enabled. Without gas phase chemistry, only a slight decrease in concentration is observed, likely caused by the dry deposition of ozone during the transport process. The decrease in the ozone concentrations near the freeway may be chiefly attributed to the reaction of ozone with high concentrations of NO near a freeway due to emission from vehicle traffic, as explained in reaction (R4.3). In addition, ozone photolysis may also partly contribute to this decrease. The observed gradual rise in ozone concentration away from the freeway is chiefly due to a decrease in NO concentration which leads to the formation of NO_2, as shown in reaction (R4.3). As the distance away from the freeway increases the concentration of NO decreases resulting in a decrease in ozone concentrations lost due to reaction (R4.3).

The sharp rise in nitric oxide concentrations near the simulated freeway, as seen in Figure 4.3(a), is chiefly due to the emission of NO from vehicles. Comparatively lower concentrations in the Case 1 (with gas phase chemistry) than in Case 2 (without chemistry) is due to the reaction of NO with ozone in Case 1 that leads to the formation of nitrogen dioxide, as explained in reaction (R4.3).

In Figure 4.3(c), it can be seen that NO_2 concentrations near the freeway are comparatively higher in Case 1 than in Case 2. This is mainly due to the formation of NO_2 from the reaction of NO with ozone, as explained in reaction (R4.3). In both cases, NO_2 changes with distance from the freeway more slowly than that of NO. This higher dilution is due to higher difference in concentration of NO produced near freeway when compared to background concentration.

In addition to NO_x and O_3, it is also interesting to look at the spatial distribution of less reactive species, CO and 1,3-Butadiene, near the freeway. CO is less reactive than 1,3-Butadiene and often used as a tracer for vehicle emissions. 1,3- Butadiene is considered a hazardous air pollutants (HAP), which could increase human cancer risk. It is selected in this study because its reaction with oxidants in the air are faster and has greater cancer risk than many other air toxics (Darnall et al. 1976) and even has greater cancer risk (Morrow 2001; Seiber 1996). These characteristics make it a better candidate to study the effect of chemistry on the spatial distribution of air toxics. As seen in Figure 4.3(d) and (e), there is a rapid increase in CO and 1,3-Butadiene concentrations at the freeway and concentrations start to fall with the distance away from freeway in both cases. There is the little change in the concentrations predicted from Case 2 due to relatively low hydroxyl radical concentration that makes the lifetime of 1,3-Butadiene near the freeway relatively long.

Hydroxyl radical (HO) is formed in the environment due to reaction of water vapor molecule with excited oxygen atom $O(^1D)$, as shown in reaction (27). In the troposphere, $O(^1D)$ is mainly produced by the photolysis of ozone. Figure 4.3(f) shows that a slight increase in the HO concentration at the freeway from the boundary concentration of 0.483 ppt to 1.14 ppt. HO_2 decreased while OH increased in this case. The relative distribution of HO and HO_2 is generally governed by the VOC/NO ratio, and this will be more clearly explained in section 4.3.6.

4.3.2. Concentration profiles at different heights

Figure 4.4 shows the concentration profiles of the species at different elevations in the domain. As discussed in the previous chapter the domain was divided into 11 layers, with finer resolution grid cells near the surface to better resolve pollutant gradients. The concentrations of each model species at the boundary of the domain at the each layer are the same as they are in the surface layer. The concentration profiles of the seven species at five layers 1, 3, 6, 9 and 11(the center of the layers are 0.5, 3, 9, 21, 35 m above surface, respectively) are shown in Figure 4-4.

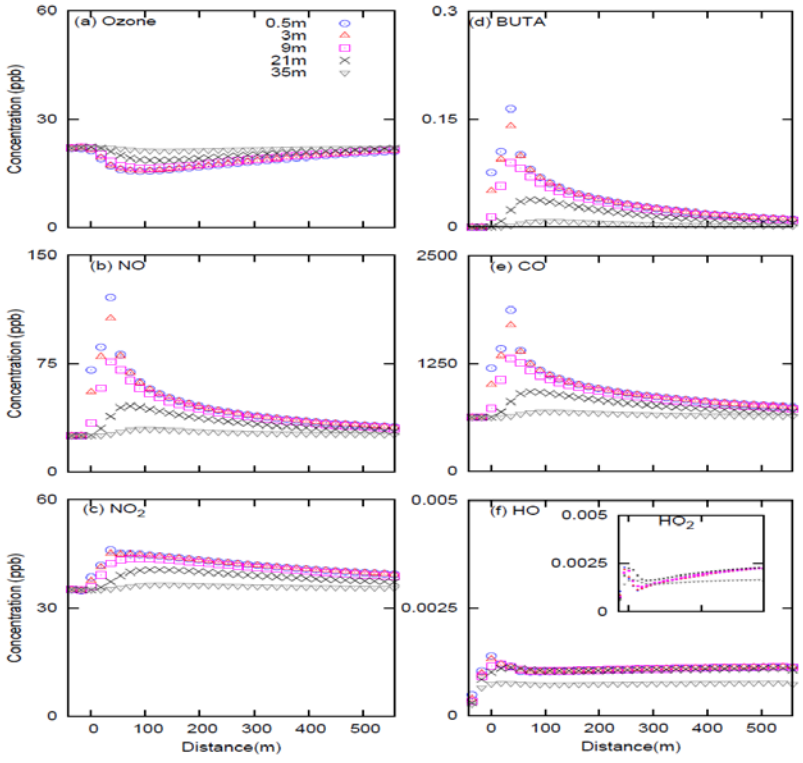

Figure 4.4 Concentration profiles of ozone, 1,3-Butadiene (BUTA), nitric oxide (NO), carbon monoxide (CO), nitrogen dioxide (NO_2), hydroxyl radical (HO) and hydroperoxy radical (HO_2), at 0.5, 3, 9, 21 and 35 m height in the model domain for Case 1.

From Figure 4.4(a), a rise in concentration of ozone at the freeway with height in the domain is observed. As explained in reaction (R4.3), reaction of ozone with nitric oxide is one of the chief contributors to the removal of ozone in a near-road environment, so the rise in ozone concentrations is due to the fall in NO concentrations at different layers, as seen in Figure 4.4(b)**.** The concentrations of NO, NO_2, CO and 1,3-Butadiene decrease with height in the domain. The fall in peak concentrations near the freeway indicate the lesser concentrations of these species that undergo a vertical transport from the surface layer where they are emitted.

In Figure 4.4(f), a fall in concentration of HO and a rise in HO_2 concentration with an increase in height in the domain are seen. This fall in peak concentrations of HO can be coupled to a relative decrease in NO concentrations when compared to a decrease in VOC concentrations with an increase in height.

4.3.3. Wind blows parallel to the freeway

Figure 4.5 shows the importance of chemistry when the wind blows parallel to the freeway. In these cases the initial concentration of species at all the layers are set to their respective boundary concentrations. Thus the time of simulation in this case was reduced by adapting a uniform concentration throughout the domain, as it reduces the time taken for the species emitted from the freeway to diffuse to other regions in the model domain. Results of two different simulations, Case 3 (with chemistry) and Case 4 (without chemistry) are shown in the figure. The results of the base case simulation are also presented in the figure for comparison purposes.

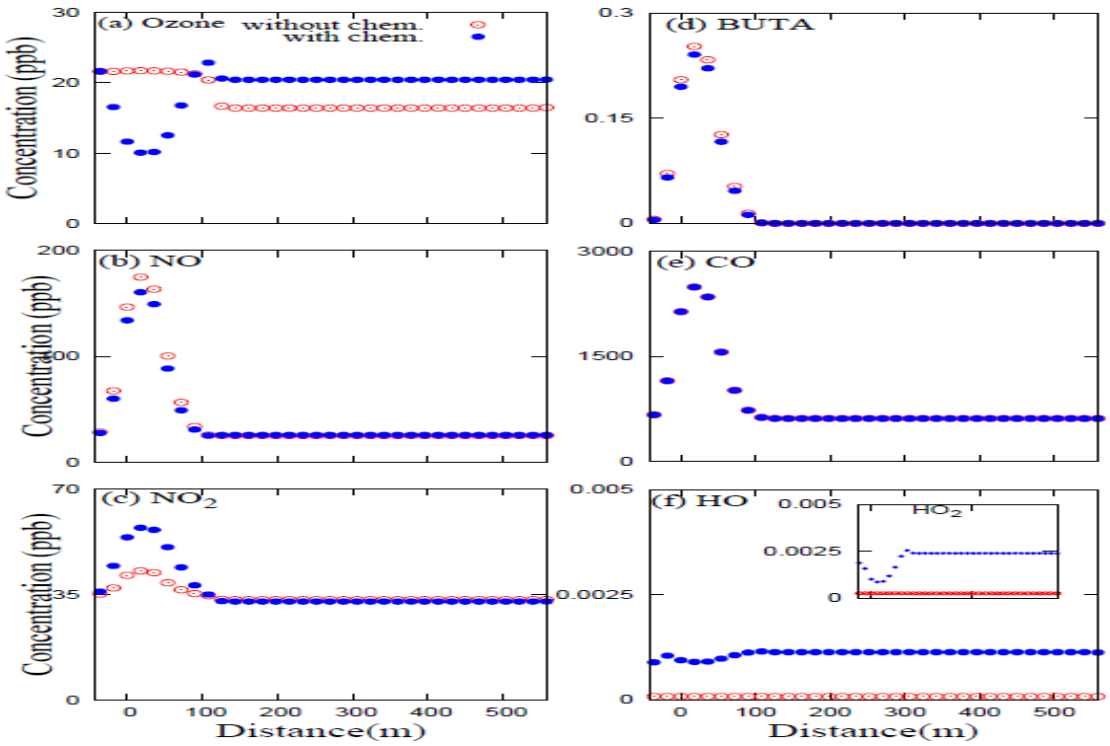

Figure 4.5 Concentration profiles of ozone, 1,3-Butadiene (BUTA), nitric oxide (NO), carbon monoxide (CO), nitrous oxide (NO_2) and radicals (HO and HO_2) for two cases case 3(with chem.) and case 4 (without chem.), at the surface layer.

Comparing Figure 4.5 (wind parallel to freeway) and Figure 4.3 (wind perpendicular to freeway) a higher concentration of species (NO_x, CO and 1-3,Butadiene) emitted from vehicles at the freeway, but lower concentrations of the same in the areas adjacent to the freeway is observed in case with wind parallel to freeway. For example, peak concentrations of NO, NO_2, CO and 1-3 Butadiene, predicted at the freeway in Case 4(without chemistry) are approximately 101, 82, 12 and 67 percent higher, than concentrations predicted from Case 2 (base case, without chemistry). This difference is attributed to higher concentrations of pollutant advecting in the direction of

freeway, when wind is parallel to freeway. The observed change in concentration profiles of the species in the Figure 4.5 are explained below.

A higher fall in concentration of ozone is observed in Figure 4.5(a) (Case 3, with chemistry), when compared to the fall observed in Figure 4.3(a) (Case 1, with chemistry). This pattern is chiefly attributed to the higher concentration profile of NO near the freeway, observed in Figure 4.5(b), as the concentration of ozone lost due to reaction with NO to form NO_2, as explained in reaction (R4.3), varies with the concentration of NO.

In Figure 4.5(b), a higher peak concentration of NO at the freeway in Case 4 (without chemistry), when compared to Case 3 (with chemistry), is observed depicting the absence of reaction of NO with ozone to form NO_2.

In Figure 4.5(c)**,** at the freeway the peak concentration of NO_2 in Case 3 (with chemistry) is about 35% than the peak concentration observed in Case 4 (without chemistry). This is higher than the difference (about 14%) of NO_2 in Figure 4.3 (c). This difference in relative concentration is due to the higher concentration of NO in Figure 4.5 which leads to NO_2 formation, as explained in reaction (R4.3).

In the Figure 4.5(f), a higher concentration of radicals, both HO and HO_2 in Case 3 (with chemistry) is predicted, when compared to Case 4 (without chemistry), which have an almost uniform concentration of 0.08 ppt and 0.26 ppt respectively and similar to boundary concentration throughout the domain. A higher fall of HO_2 at the freeway in subplot of Figure 4.5(f), when compared to the fall in Figure 4.3(f) is observed. This

higher fall can be explained by fall in VOC/NO ratio observed in the figure in section 4.3.6.

4.3.4. High ozone boundary condition simulation

Figure 4.6 shows the spatial distribution of species in the regions where higher ozone boundary concentrations are observed. Results of simulation for two different cases Case 5 (with chemistry) and Case 6 (without chemistry) are shown.

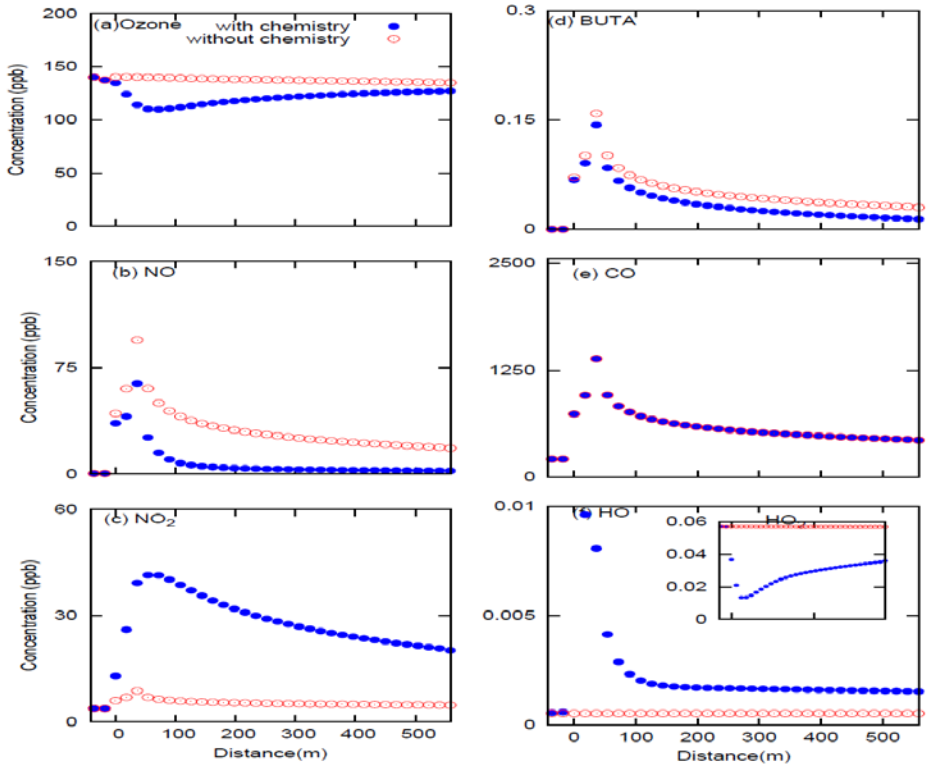

Figure 4.6 Concentration of ozone, 1,3-Butadiene (BUTA), nitric oxide (NO), carbon monoxide (CO), nitrogen dioxide (NO_2), hydroxyl radicals (HO) and hydroperoxy radical (HO_2) with higher boundary concentration of ozone (Cases 5 and 6).

The concentration profiles of each species observed in the Figure 4.6 is discussed below.

From Figure 4.3(b) and Figure 4.6(b), a greater fall in peak NO concentrations in Case 5 (with chemistry, higher boundary ozone) than in Case 1 (with chemistry, base case boundary ozone), compared to their corresponding cases Case 6 and Case 2 is seen. This higher difference can be attributed to higher ozone concentrations in Case 6 and Case 5 which instigate the formation of NO_2 from NO, as shown in reaction (R4.3). Similarly, a greater rise in concentration of NO_2 at the freeway of about 300% in Case 5 (with chemistry) in Figure 4.6(c)**,** when compared to rise of about 13% in Case1 (base case, with chemistry) in Figure 4.3(c). This change can be attributed to higher ozone concentrations which lead to a higher depletion of NO and a higher formation of NO_2 as explained by reaction (R4.3).

An interesting scenario is observed in Figure 4.6(f). A higher difference in concentration of HO_2 radical is observed at the freeway in Case 5 (with chemistry) when compared to Case 6 (without chemistry), compared to difference observed in sub plot of Figure 4.3(f). The boundary concentration of HO_2 has also increased by a factor of 10, when compared to the Case 1 (base case, with chemistry). This increase in boundary concentration can be explained by higher ozone and higher VOC/NO ratio in the boundary of the domain as seen in Figure 4.8 and explained in the section 4.3.6.

Similarly a higher rise in concentration of HO is observed in Figure 4.6(f) (approximately 7.5 ppt), compared to Figure 4.3(f) (approximately 0.9 ppt). This can be attributed to a relative rise in NO concentrations when compared to rise in VOC near a

freeway, as seen in Figure 4.8. It is also interesting to see a higher concentration range for HO_2 when compared to HO throughout the domain, when compared to Case 1 (Base case) or Case 7 (with higher diesel fraction), where almost similar concentration ranges are observed. This higher range of HO_2 is due to higher VOC/NO ratio when compared to the base case, as explained in section 4.3.6.

Higher concentration of HO radicals in Case 5 (with chemistry) , when compared to concentrations predicted in Case 1 (base case, with chemistry) lead to a higher difference (about 11 %) in peak concentrations of 1,3-Butadiene in Figure 4.6(d) in cases with and without chemistry, when compared to just 1% difference in Figure 4.3(d)(base case).

4.3.5. Higher diesel fraction

Figure 4.7 shows the concentration profiles of species when the fleet comprises of a higher fraction of diesel powered vehicles. The simulation results of Case 7(with chemistry) and Case 8(without chemistry) are shown in this figure.

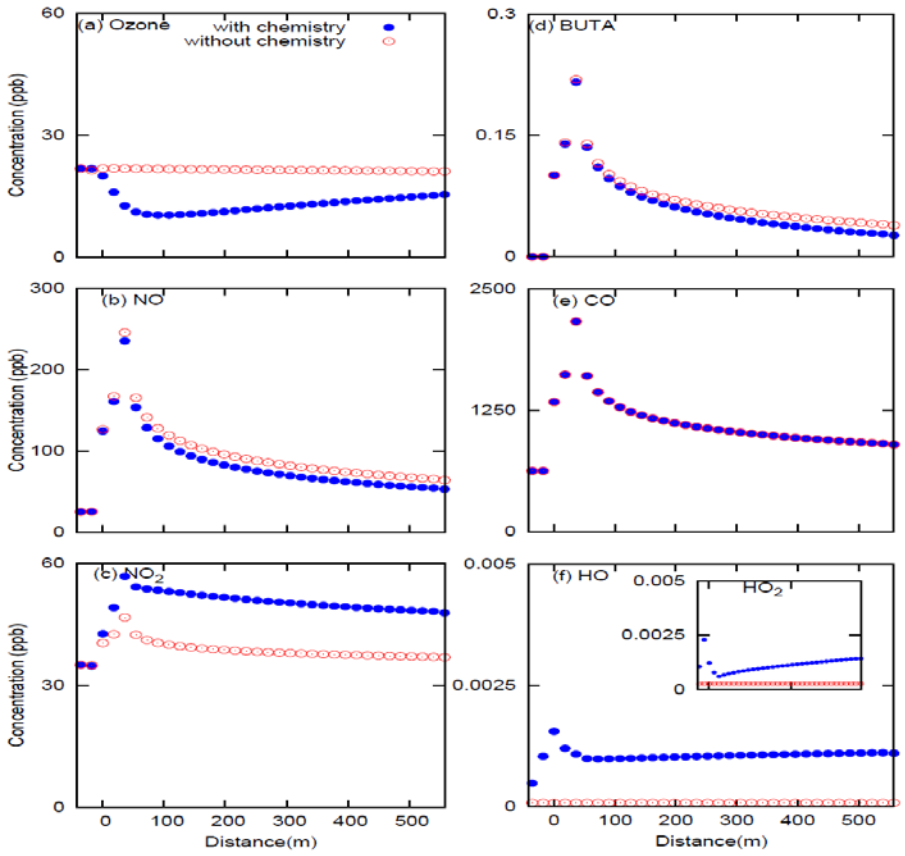

Figure 4.7 Concentration of ozone, 1,3-Butadiene (BUTA), nitric oxide (NO), carbon monoxide (CO), nitrogen dioxide (NO_2), hydroxyl radicals (HO) and per-hydroxyl radical (HO_2) for the cases with higher diesel fraction in vehicle fleet (Cases 7 and 8).

As diesel vehicles produce more NO_x than gasoline vehicles, the peak concentrations of NO_x observed in Case 7 and 8 are higher than those of the base case (Case 1 and 2). For example, peak concentrations of NO and NO_2 in Case 8 (without chemistry) are about 94% and 15% higher than their corresponding peak concentrations predicted in Case 2 (base case, without chemistry). A higher increase in NO_2 observed in Case 7 (with chemistry, higher diesel fraction) in Figure 4.7, when compared to rise in

Case 1 (with chemistry, base case) in Figure 4.3 is due to higher concentrations of NO, as explained in reaction (R4.3).

From Figure 4.3(a) and Figure 4.7(a), a greater fall in concentration of ozone is predicted in case with higher diesel fraction (Case 7, with chemistry) than in the Case1 (base case, with chemistry). This extra fall can be attributed to the higher NO concentration in Case 7 and 8, when compared their corresponding the base cases (Case 1 and 2), because the removal mechanism of ozone is its reaction with NO, as explained in reaction (R4.3).

A slight increase in HO concentration and a slight decrease in HO_2 concentrations in Case 7 (with chemistry) in Figure 4.7(f) are seen. This change is due to lower VOC/NO ratio observed in Case 7 (with chemistry, high diesel) when compared to Case 1 (with chemistry, base case), as explained in section 4.3.6.

An increase in concentration peaks of CO and 1,3-Butadiene by about 15% and 30% respectively in Case 8 (without chemistry) when compared to case 2 (base case, without chemistry) is observed. This rise can be attributed to the increase in diesel powered engines in vehicle fleet. A slight higher fall in 1-3 Butadiene in case where chemistry is included in Figure 4.7(d) when compared to Case 1 (with chemistry, base case) in Figure 4.3(d) is due to slight higher OH concentrations observed in Figure 4.7(f) when compared to the later.

4.3.6. Factors affecting HO and HO_2 concentration

Levy (1971) used reactions R4.1-R4.12 and showed that in normal atmosphere the steady state relation between HO_2 and OH can be given by (4.16),(4.17) and (4.18)

$$\frac{\left[HO_2^{\cdot}\right]}{\left[HO^{\cdot}\right]} = \frac{k_{OH^{\cdot}-RH}[RH]}{k_{HO_2^{\cdot}-NO}\left[NO\right]} \tag{4.16}$$

$$\left[HO_2^{\cdot} + HO^{\cdot}\right] = \sqrt{\frac{2k_{O\left(^1D\right)-H_2O}\left[O\left(^1D\right)\right]\left[H_2O\right]}{k_{OH-OH}}} \tag{4.17}$$

$$\left[HO^{\cdot}\right] = \left(\frac{\sqrt{\frac{2k_{O\left(^1D\right)-H_2O}\left[O\left(^1D\right)\right]\left[H_2O\right]}{k_{OH-OH}}}}{1+\frac{k_{OH^{\cdot}-RH}[RH]}{k_{HO_2^{\cdot}-NO}\left[NO\right]}}\right) \tag{4.18}$$

From equation (4.16), we observe that in a system at steady state the ratio of HO_2 to OH chiefly depends on the ratio of VOC to NO, i.e. an increase in VOC/NO results in an increase in HO_2/HO and vice versa. From Equation (4.17), it can be seen that the overall HO_x concentration is proportional to the $O(^1D)$ concentration, thus it is proportional to ozone concentration. Equation (4.18) can be derived by combining Equation (4.16) and (4.17). It can be seen that two factors affect the HO_x concentration, ozone and VOC/NO ratio. HO concentration is proportional to the ozone concentration and inversely proportional to VOC/NO ratio. Depending on the ratios of RH-HO reaction rate and the NO-HO_2 rate, the effect of VOC/NO ratio on HO concentration can vary.

Figure 4.8 shows the ratio of VOC and NO throughout the domain for Case 1 (base case), Case 3 (with wind parallel to freeway), Case 5 (with higher ozone boundary concentration) and Case 7 (with higher diesel fraction in vehicle fleet).

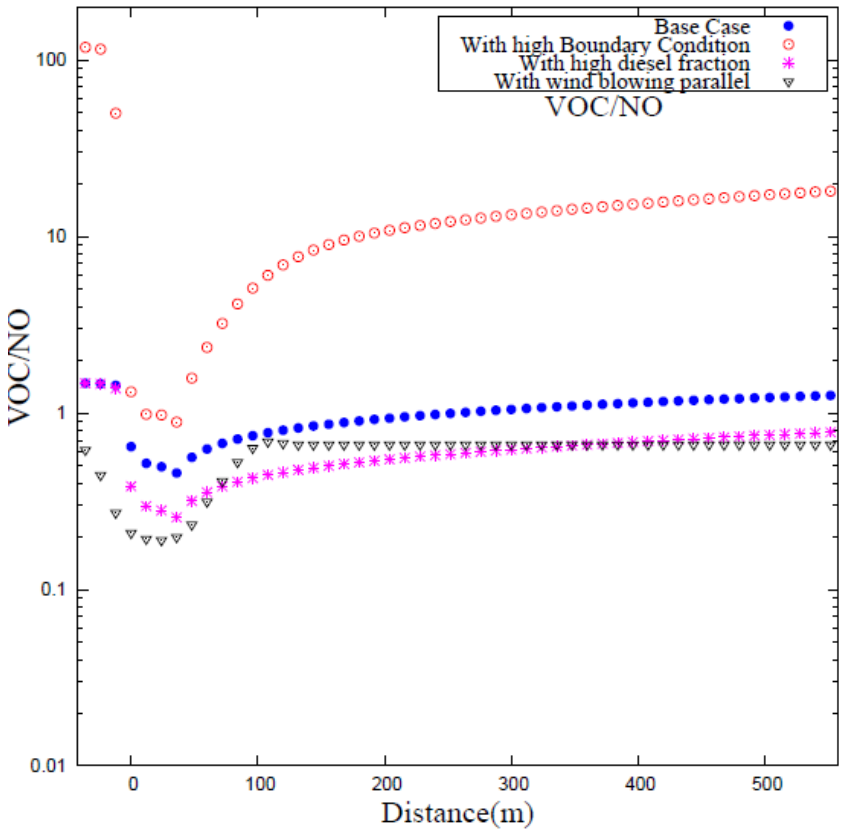

Figure 4.8 VOC to NO ratio for four different cases Cases 1, 3, 5 and 7. '0' on the X-axis indicated the starting point of the freeway.

From Figure 4.8 a fall in VOC to NO at freeway region (i.e. 0 to 36 m on X-axis) is observed in all the cases. This shows the relative higher concentration of NO when compared to VOC emitted from a vehicle exhaust. The decrease in the VOC/NO ratio qualitatively explains the increase in the HO concentration. The VOC/NO ratio for Case 5 (with higher ozone boundary condition case) is slightly higher than Case 1 (Base case) and this can be attributed to higher ozone and lower NO being available at the boundary. A lower VOC/NO is observed in Case 7 (with higher diesel fraction) when compared to Case 1(base case). This is attributed to the increase in diesel fraction in vehicle fleet

which emits high NO when compared to a gasoline vehicle. The high ozone concentration explains why the highest HO concentration occurs in Case 5 near the freeway. The significant HO decrease in that case is well predicted by the sharp decrease in the VOC/NO ratio.

4.4. Summary

The cases studied in the chapter suggests that gas phase chemistry is needed to accurately predict the concentration of ozone, NO, NO_2 and 1,3-Butadiene near a busy freeway. The effect of gas phase chemistry on 1,3-Butadiene is less significant when the freeway is in a ozone depleted location such as in the urban center, but is quite significant when the freeway is located in a location downwind of the urban ozone plume due to a significant increase in the HO radical concentration. Neglecting the gas chemistry near freeway will lead to an overestimation ozone-rich of the air toxics concentrations in the downwind direction. In addition, the increase in the HO radical near the freeway may also imply potential health effects due to the strong oxidative power of the radicals.

CHAPTER V

SUMMARY AND SCOPE OF FUTURE RESEARCH

5.1. Summary

This study developed a new near-road air quality model which incorporated a modern gas phase chemistry to study the air quality in an urban area. A detailed description of the model developed was presented. Two kinds of simulations were run using the model. In the first simulation, the transport mechanism of the model was validated using an already acclaimed data set. Statistical analysis of the performance of the model and its comparison with other near-road models was explained. The validated model was used to study the concentration profiles of gaseous species near a simulated freeway at Houston.

5.2. Scope of Future Research

The following are the recommendations for future research:

1. To further study pollutant dispersion and reaction near freeways using computational fluid dynamics (CFD) approach.
2. To get real time data to validate the chemical mechanism of the model.
3. To develop the model so that it can be used to study particulate matter.
4. To study the performance of the model at an urban area with a multiple freeway links.

REFERENCES

Balmes, J. R., Earnest, G., Katz, P. P., Yelin, E. H., Eisner, M. D., Chen, H., Trupin, L., Lurmann, F., and Blanc, P. D. (2009). "Exposure to traffic: Lung function and health status in adults with asthma." *Journal of Allergy and Clinical Immunology*, 123(3), 626-631.

Bäumer, D., Vogel, B., and Fiedler, F. (2005). "A new parameterisation of motorway-induced turbulence and its application in a numerical model." *Atmospheric Environment*, 39(31), 5750-5759.

Benson, P. E. (1992). "A review of the development and application of the CALINE3 and 4 models." *Atmospheric Environment. Part B. Urban Atmosphere*, 26(3), 379-390.

Brugge, D., Durant, J., and Rioux, C. (2007). "Near-highway pollutants in motor vehicle exhaust: A review of epidemiologic evidence of cardiac and pulmonary health risks." *Environmental Health*, 6(1), 23.

Cadle, S. H., Chock, D. P., Heuss, J. M., and Monson, P. R. (1976). "Results of the General Motors sulfate dispersion experiment." General Motors Research Laboratories, Warren ,MI.

Carter, W. P. L. (2000). "Implementation of the SAPRC-99 chemical mechanism into the models-3 framework." US Environmental Protection Agency, Washington, DC.

Corlella, P., and Woodward, P. R. (1984). "Piecewise parabolic method (PPM) for gas-dynamical simulations." *J. Comput. Phys.*, 54(1), 174-201.

Darnall, K. R., Lloyd, A. C., Winer, A. M., and Pitts, J. N. (1976). "Reactivity scale for atmospheric hydrocarbons based on reaction with hydroxyl radical." *Environmental Science & Technology*, 10(7), 692-696.

Finkelstein, M. M., Jerrett, M., and Sears, M. R. (2004). "Traffic air pollution and mortality rate advancement periods." *Am. J. Epidemiol.*, 160(2), 173-177.

Gauderman, W. J., Vora, H., McConnell, R., Berhane, K., Gilliland, F., Thomas, D., Lurmann, F., Avol, E., Kunzli, N., Jerrett, M., and Peters, J. (2007). "Effect of exposure to traffic on lung development from 10 to 18 years of age: A cohort study." *The Lancet*, 369(9561), 571-577.

Grosjean, D., Grosjean, E., and Gertler, A. W. (2001). "On-road emissions of carbonyls from light-duty and heavy-duty vehicles." *Environmental Science & Technology*, 35(1), 45-53.

Held, T., Chang, D. P. Y., and Niemeier, D. A. (2003). "UCD 2001: An improved model to simulate pollutant dispersion from roadways." *Atmospheric Environment*, 37(38), 5325-5336.

Holmes, N. S., and Morawska, L. (2006). "A review of dispersion modelling and its application to the dispersion of particles: An overview of different dispersion models available." *Atmospheric Environment*, 40(30), 5902-5928.

Jacobson, M. Z. (2005). *Fundamentals of atmospheric modeling*, Cambridge University Press, Cambridge, UK.

Kean, A. J., Harley, R. A., Littlejohn, D., and Kendall, G. R. (2000). "On-road measurement of ammonia and other motor vehicle exhaust emissions." *Environmental Science & Technology*, 34(17), 3535-3539.

Kim, J. J., Smorodinsky, S., Lipsett, M., Singer, B. C., Hodgson, A. T., and Ostro, B. (2004). "Traffic-related air pollution near busy roads: The east bay children's respiratory health study." *Am. J. Respir. Crit. Care Med.*, 170(5), 520-526.

Kinnee, E. J., Touma, J. S., Mason, R., Thurman, J., Beidler, A., Bailey, C., and Cook, R. (2004). "Allocation of onroad mobile emissions to road segments for air toxics modeling in an urban area." *Transportation Research Part D: Transport and Environment*, 9(2), 139-150.

Levy, H., II. (1971). "Normal atmosphere: Large radical and formaldehyde concentrations predicted." *Science*, 173(3992), 141-143.

McRae, G. J., Goodin, W. R., and Seinfeld, J. H. (1982). "Development of a second-generation mathematical model for urban air pollution--I. Model formulation." *Atmospheric Environment (1967)*, 16(4), 679-696.

Monin, A., and Obukhv, A. (1954). "Basic laws of turbulent mixing in the ground layer of the atmosphere." *Akad. Nauk, SSSR, Geo fiz.Inst. Trudy.*, 151, 163-187.

Morrow, N. L. (2001). "Significance of 1,3-butadiene to the US air toxics regulatory effort." *Chemico-Biological Interactions*, 135-136, 137-143.

Murena, F. (2007). "Air quality nearby road traffic tunnel portals: BTEX monitoring." *Journal of Environmental Sciences*, 19(5), 578-583.

Niemeier, U., Granier, C., Kornblueh, L., Walters, S., and Brasseur, G. P. (2006). "Global impact of road traffic on atmospheric chemical composition and on ozone climate forcing." *J. Geophys. Res.*, 111.

Ntziachristos, L., Ning, Z., Geller, M. D., Sheesley, R. J., Schauer, J. J., and Sioutas, C. (2007). "Fine, ultrafine and nanoparticle trace element compositions near a major freeway with a high heavy-duty diesel fraction." *Atmospheric Environment*, 41(27), 5684-5696.

Press W.H, Flannery B. P., Teukolsky S.A,Vetterling W.T. (1992). *Numerical recipes in Fortran: The art of scientific computing*, II Ed., Cambridge University Press, New York.

Rao, K. S. (2002). "ROADWAY-2: A model for pollutant dispersion near highways." *Water, Air, & Soil Pollution: Focus*, 2(5), 261-277.

Rao, S. T., Sistla, G., Eskridge, R. E., and Petersen, W. B. (1986). "Turbulent diffusion behind vehicles: Evaluation of ROADWAY models." *Atmospheric Environment (1967)*, 20(6), 1095-1103.

Richmond-Bryant, J., Saganich, C., Bukiewicz, L., and Kalin, R. (2009). "Associations of PM2.5 and black carbon concentrations with traffic, idling, background pollution, and meteorology during school dismissals." *Science of The Total Environment*, 407(10), 3357-3364.

Sahlodin, A. M., Sotudeh-Gharebagh, R., and Zhu, Y. (2007). "Modeling of dispersion near roadways based on the vehicle-induced turbulence concept." *Atmospheric Environment*, 41(1), 92-102.

Sehmel, G. A. (1973). "Particle resuspension from an asphalt road caused by car and truck traffic." *Atmospheric Environment*, 7(3), 291-309.

Seiber, J. N. (1996). "Toxic air contaminants in urban atmospheres: Experience in California." *Atmospheric Environment*, 30(5), 751-756.

Seinfeld, J. H., and Pandis, S. N. (2006). *Atmospheric chemistry and physics: From air pollution to climate change*, Wiley-Interscience, Hoboken, New Jersey, US.

Stull. (1988). *An introduction to the boundary layer meteorology*, Kluwer Academic Publishers, Boston.

USEPA. (2009). "US Greenhouse gas emission inventory report." U.S. Environmental Protection Agency, Washington, D.C.

Venkatram, A. (2004). "On estimating emissions through horizontal fluxes." *Atmospheric Environment*, 38(9), 1337-1344.

Venkatram, A., Isakov, V., Thoma, E., and Baldauf, R. (2007). "Analysis of air quality data near roadways using a dispersion model." *Atmospheric Environment*, 41(40), 9481-9497.

Venn, A. J., Lewis, S. A., Cooper, M., Hubbard, R., and Britton, J. (2001). "Living near a main road and the risk of wheezing illness in children." *Am. J. Respir. Crit. Care Med.*, 164(12), 2177-2180.

Wade, J., Holman, C., and Fergusson, M. (1994). "Passenger car global warming potential: Current and projected levels in the UK." *Energy Policy*, 22(6), 509-522.

Young, T. R., and Boris, J. P. (1977). "A numerical technique for solving stiff ordinary differential equations associated with the chemical kinetics of reactive-flow problems." *The Journal of Physical Chemistry*, 81(25), 2424-2427.

Zhu, Y., Hinds, W. C., Kim, S., Shen, S., and Sioutas, C. (2002). "Study of ultrafine particles near a major highway with heavy-duty diesel traffic." *Atmospheric Environment*, 36(27), 4323-4335.

APPENDIX A

FLOW CHART EXPLAINING THE MODEL MECHANISM

FLOW CHART

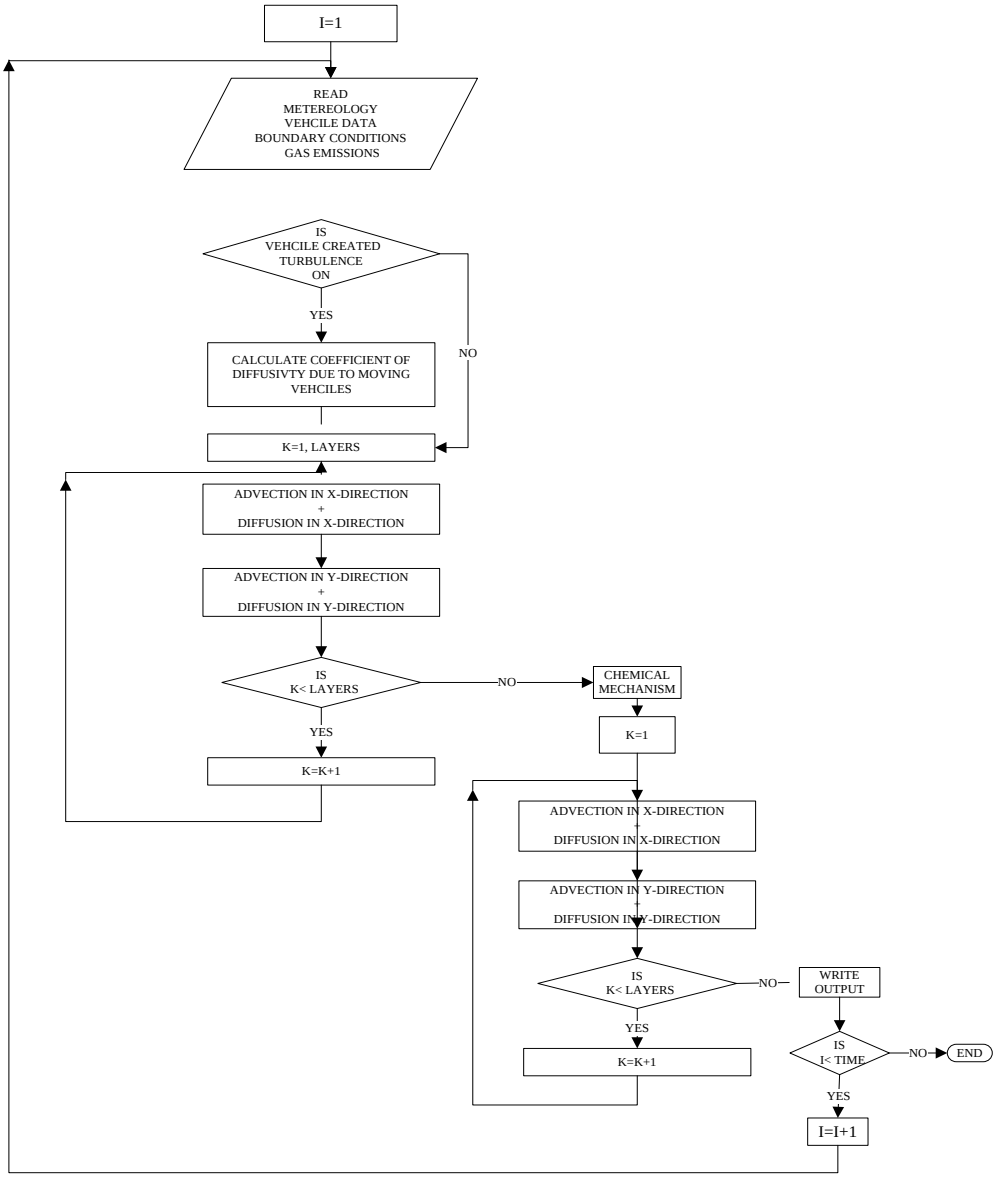

APPENDIX B

LIST OF SPECIES INCLUDED IN THE CHEMICAL MECHANISM

Table B: List of species in the chemical mechanism(Carter 2000)

O3	PROD2	RO2-R.
NO	RNO3	R2O2.
NO2	DCB1	RO2-N.
HO.	DCB2	CCO-O2.
HONO	DCB3	PAN
CO	ALK1	RCO-O2.
SO2	ALK2	PAN2
HCHO	ALK3	BZCO-O2.
CCHO	ALK4	PBZN
RCHO	ALK5	MA-RCO3.
ACET	ARO1	MA-PAN
MEK	ARO2	MACR
MEOH	OLE1	IPROD
COOH	OLE2	ETHENE
ROOH	SULF	ISOPRENE
GLY	SF6	TERP
MGLY	NO3	NH3
BACL	N2O5	HCL
PHEN	HNO3	C2H2
CRES	HO2.	MTBE
NPHE	HNO4	BENZ
BALD	HO2H	BUTA
MVK	C-O2.	ACROLEIN

APPENDIX C

AN EXAMPLE RUNSCRIPT USED FOR MOBILE6 INPUT

AN EXAMPLE RUNSCRIPT USED AS AAN INPUT TO RUN MOBILE6

******** HEADER **********

MOBILE6 INPUT FILE:

POLLUTANTS : HC NOX CO

AIR TOXICS :

PARTICULATES :

DATABASE OUTPUT :

DATABASE VEHICLES : 22222 22222222 2 222 22222222 222

DATABASE HOURS : 12,12

*WITH FIELDNAMES :

******** RUN 1 **********

RUN DATA :

EXPRESS HC AS TOG :

FUEL RVP : 8.7

EXPAND EXHAUST :

******** SCENARIO 1 *********

SCENARIO RECORD : RUN 1 SCE 1

CALENDAR YEAR : 2000

EVALUATION MONTH : 7

AVERAGE SPEED : 60 freeway

MIN/MAX TEMP : 90 90

RELATIVE HUMIDITY : 50 50 50 50 50 50 50 50 50 50 50 50

50 50 50 50 50 50 50 50 50 50 50 50

PARTICULATE EF : PMGZML.CSV PMGDR1.CSV PMGDR2.CSV PMDZML.CSV PMDDR1.CSV PMDDR2.CSV

PARTICLE SIZE : 10.0

DIESEL SULFUR : 395

GASOLINE SULFUR : 300

E200 : 50

E300 : 100

OXYGENATE : MTBE 15.1 0.50

: ETBE 17.6 0.05

: ETOH 10.0 0.45

: TAME 6.0 0.00

GAS BENZENE% : 1.5

GAS OLEFIN% : 15

GAS AROMATIC% : 15

******** END OF RUN *******

VITA

Name:	Sri Harsha Kota, EIT
Permanent Address:	205, WERC, Zachry Dept. of Civil Engineering, Texas A&M University, 3136 TAMU, College Station, Texas, 77843-3136
Education:	B.E. Civil Engineering Chaitanya Bharathi Institute of Technology, India 2007 M.S. Civil Engineering Texas A&M University, College Station 2009
Member:	American Society of Civil Engineers
Email Address:	harshakota@gmail.com